Soil Dynamics and Earthquake Engineering 82 (2016) 222–240

Contents lists available at ScienceDirect

Soil Dynamics and Earthquake Engineering

journal homepage: www.elsevier.com/locate/soildyn

InterPACIFIC project: Comparison of invasive and non-invasive methods for seismic site characterization. Part I: Intra-comparison of surface wave methods

F. Garofalo [a,1], S. Foti [a,*], F. Hollender [b], P.Y. Bard [c], C. Cornou [c], B.R. Cox [d], M. Ohrnberger [e], D. Sicilia [f], M. Asten [g], G. Di Giulio [h], T. Forbriger [i], B. Guillier [c], K. Hayashi [j], A. Martin [k], S. Matsushima [l], D. Mercerat [m], V. Poggi [n], H. Yamanaka [o]

[a] Politecnico di Torino, Torino, Italy
[b] French Alternative Energies and Atomic Energy Commission (CEA), Cadarache, Saint-Paul-lez-Durance, France
[c] Univ. Grenoble Alpes/CNRS/IRD/IFSTTAR, ISTerre, F-38000 Grenoble, France
[d] University of Texas, Austin, TX, USA
[e] University of Potsdam, Potsdam, Germany
[f] EdF, France
[g] Monash University, Melbourne, Australia
[h] INGV, L'Aquila, Italy
[i] Black Forrest Observatory, Germany
[j] Geometrics, USA
[k] Geovision, USA
[l] Kyoto University, Japan
[m] CEREMA, Direction Territoriale Méditerranée, Nice, France
[n] Swiss Seismological Service, ETHZ, Zurich, Switzerland
[o] Tokyo Institute of Technology, Japan

ARTICLE INFO

Article history:
Received 19 June 2015
Received in revised form
6 December 2015
Accepted 17 December 2015
Available online 21 January 2016

Keywords:
Surface-wave methods
Dispersion curve
Inversion
$V_{S,30}$
Site characterization
MASW
Microtremors
Rayleigh waves
Geophysical methods

ABSTRACT

The main scope of the InterPACIFIC (Intercomparison of methods for site parameter and velocity profile characterization) project is to assess the reliability of in-hole and surface-wave methods, used for estimating shear wave velocity. Three test-sites with different subsurface conditions were chosen: a soft soil, a stiff soil and a rock outcrop. This paper reports the surface-wave methods results. Specifically 14 teams of expert users analysed the same experimental surface-wave datasets, consisting of both passive and active data. Each team adopted their own strategy to retrieve the dispersion curve and the shear-wave velocity profile at each site. Despite different approaches, the dispersion curves are quite in agreement with each other. Conversely, the shear-wave velocity profiles show a certain variability that increases in correspondence of major stratigraphic interfaces. This larger variability is mainly due to non-uniqueness of the solution and lateral variability. As expected, the observed variability in $V_{S,30}$ estimates is small, as solution non-uniqueness plays a limited role.

1. Introduction

The shear wave velocity (V_S) model plays a key role in seismic site response analysis, since shear wave propagation controls ground motion amplification [1,2]. Seismic building codes, such as Eurocode 8 [3] and NERHP Provisions [4], use $V_{S,30}$ (i.e. the time-averaged velocity in the topmost 30 m) to define soil classes for simplified assessment of seismic site response. Also, most modern GMPEs (Ground Motion Prediction Equations) used in seismic hazard evaluation consider $V_{S,30}$ as a parameter to bin sites on the basis of expected site amplification [5–8]. An accurate study of the seismic response can be derived from numerical methods, and in this case, a 1D, 2D or 3D distribution of V_S is required.

The V_S model can be retrieved either with invasive tests, such as cross-hole or down-hole tests, or non-invasive methods, such as surface-wave methods or refraction tests. Invasive methods are

* Correspondence to: Corso Duca degli Abruzzi, 24, 10129 Torino, Italy.
E-mail address: Sebastiano.foti@polito.it (S. Foti).
[1] Currently at Eni upstream and technical services, Italy.

http://dx.doi.org/10.1016/j.soildyn.2015.12.010
0267-7261/

generally considered more reliable than non-invasive methods because they are based on the interpretation of local measurements of shear-wave traveltimes, providing generally a good resolution as a function of depth. However, invasive methods require the drilling of at least one borehole, making them quite expensive for obtaining deep information. Hence, they are usually adopted only in projects of relevant importance. Non-invasive techniques provide cost efficient alternatives. Specifically, methods based on the analysis of surface wave propagation are increasingly more and more popular [9–14]. Surface-wave methods require usually little efforts for field acquisition. However, they require processing and inversion of the experimental data that are much more computationally intensive than those required for invasive methods. While the processing of the dispersion curve is quite robust as discussed by Cornou et al. [15] and Cox et al. [16], the surface-wave inversion problem, used to obtain a V_S profile, is highly non-linear and affected by solution non-uniqueness. These factors can induce interpretation ambiguities on the final V_S model [17–25]. In literature, different techniques for both dispersion processing, (e.g., [26–31]) and inversion (e.g., [21,32–39]) of the experimental data have been proposed. These techniques can be considered reliable if expert users apply them. However, because of the low cost and time effectiveness of surface wave methods and the availability of "black-box" software, non-expert users are increasingly adopting these methods. Uncorrected interpretation of the surface-wave data may lead to large errors in the resulting V_S profile, generating sometimes a lack of confidence in non-invasive methods.

In the past, several projects were carried out to improve the overall state-of-practice in surface-wave methods, like the NERIES-JRA4 European project (NEtwork of Research Infrastructures for European Seismology) [9]. In 2006, an international blind test [15] was conducted, but this was mainly focused on ambient vibration array recordings. Asten et al. [40] report a blind comparison of five independent interpretations of ambient vibrations, at two sites in basins on the North Anatolian Fault, Turkey. Tran and Hiltunen [41] compared results obtained by 10 independent teams who analysed the same experimental dataset collected with linear arrays recording active-source data and ambient vibrations. Kim et al. [42] report on a local blind test with independent measurements and analysis of surface wave data at a site with shallow bedrock in which variability of borehole methods was also investigated. Cox et al. [16] proposed a blind test, in which the participants analysed the same dataset of both passive and active surface-wave records, aimed at assessing the uncertainty/variability in both dispersion and V_S estimations. Unfortunately, the lack of in-hole tests did not allow an independent assessment of accuracy of the prediction at the site considered in this blind test.

In this context, the InterPACIFIC (Intercomparison of methods for site parameter and velocity profile characterization) project is aimed at comparing the main techniques for surface-wave methods (intra-method comparisons), as well as comparing non-invasive techniques with invasive ones (inter-method comparisons) at three European sites with different subsurface conditions. In this paper we report only the intra-method comparison among the surface-wave results in order to evaluate the reliability of surface-wave methods. The inter-methods comparison between surface-wave methods and in-hole techniques is discussed in a companion paper [43]. This intra-method comparison of surface-wave results will help us to improve the understanding of those issues that could impact the reliability of site characterization results.

The three test-sites selected within the interPACIFIC project (Fig. 1) are characterized by different subsurface conditions: a site with soft soil overlying rock (Mirandola); a site with stiff soil extending to significant depths (Grenoble); a rock outcrop site (Cadarache). The Mirandola site is located in Italy near the epicentral area of the 2012 Emilia seismic sequence [44], and consists of approximately 100 m of soft alluvial soil overlying rock. The Grenoble site is situated in an Alpine valley in France, and consists of very deep, stiff alluvial deposits from about 500–800 m [45]. The Cadarache site, also in France, is a rock outcrop site. At all of the sites, invasive (in-hole) measurements were performed (at least two boreholes were available) while surface-wave data were acquired in the vicinity of the boreholes.

Fourteen expert teams (engineers, geologists and seismologists) from different institutions/companies (see Table 1), were invited to take part at a blind test in surface wave analysis. The same experimental non-invasive datasets were provided to all of the teams. Each team was allowed to use all or part of the data provided. Very little supplemental information was provided about the sites.

Each team was free to adopt the strategy and the procedure they considered the best to estimate a V_S profile for the site, with no specific requirements on investigation depth and resolution. In order to take into account the issue of non-uniqueness of the solution, the teams were required to provide both their best estimate of the V_S profile and an associated uncertainty bound (or a range of possible solutions). Nevertheless, a comparison of the uncertainty bounds is not straightforward, as the non-uniqueness is quantified with several different strategies by the analysts.

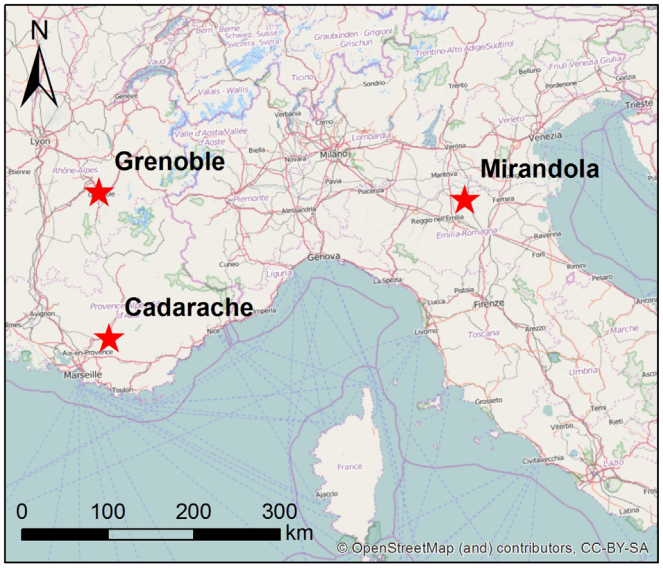

Fig. 1. Localization of the three sites: Mirandola in Italy, Grenoble and Cadarache in France.

Table 1
List of teams participating in the surface-wave analysis blind exercise.

ID	Label	Participants	Country
1	MU	Michael Asten, Monash University	Australia
2	CE	Diego Mercerat, CEREMA	France
3	IST1	Cécile Cornou, ISTerre	France
4	UT	Brady Cox, University of Texas	USA
5	INGV	Giuseppe Di Giulio, INGV	Italy
6	BFO	Thomas Forbriger, Black Forest Observatory	Germany
7	Geom	Koichi Hayashi, Geometrics	USA
8	IST2	Bertrand Guillier, ISTerre	France
9	KU	Shinichi Matsushima, Kyoto University	Japan
10	TT	Hiroaki Yamanaka, Tokyo Institute of Technology	Japan
11	GV	Antony Martin, Geovision	USA
12	SED	Valerio Poggi, Stefano Maranò, Jan Burjanek, Clotaire Michel, SED-ETHZ	Switzerland
13	PU	Matthias Ohrnberger, Potsdam University	Germany
14	PT	S. Foti and F. Garofalo, Politecnico di Torino	Italy

Hence, the present paper is focused on the comparison of the best estimates only. There is not a unique definition of best estimate, and each team decided their preferred strategy (lowest misfit, by eye, statistics on solutions, …) for providing their profile.

The paper is organized as follows. After a brief introduction on the surface-wave techniques, we describe the acquisition of the experimental data (common to the teams within the blind test) and the approaches for their interpretation as adopted by the different teams. Then, for each site, a brief description of the subsurface conditions and the comparison of the results are reported. Finally, the results are discussed to summarize the important lessons learned.

2. Surface wave methods

Surface-wave methods are based on the estimation and inversion of the dispersive characteristic of the site. Surface wave propagation is a phenomenon that occurs in the case of a free boundary, such as the surface of the earth. In a homogeneous medium, the amplitude of induced particle motion decays exponentially with depth, becoming negligible within about one wavelength. In a layered medium, surface-wave propagation is governed by geometric dispersion: different wavelengths investigate different depths and, hence, at each frequency the phase velocity depends on the properties of the investigated portion of the subsurface. The phase velocity as a function of frequency or wavelength is called a dispersion curve. Moreover, in a layered medium, the surface-wave propagation is a multimodal phenomenon, wherein different modes of vibration can exist at each frequency, and each mode is characterized by its own propagation velocity [44]. However, in a normally dispersive profile (velocity consistently increasing with depth) with no strong impedance contrasts, the energy tends to propagate primarily according to the fundamental mode [46–48]. The dispersion curve of the fundamental mode is usually estimated but also higher modes can be identified. Others prefer to estimate the effective mode, that utilizes the theoretical energy partition between modes for a given model, assuming sources are vertical-impact point sources [49,50].

In practice, most surface-wave methods are based on three main steps: the data acquisition, the processing to extract the dispersion curve and finally the inversion [49,50,51,13].

2.1. Acquisition

Surface-wave analysis can be implemented on active-source and/or passive-source tests. For the former, the wave is specifically generated for the experiment, whereas for the latter ambient noise vibrations (microtremors) are recorded. It is important to highlight that the signals related to active and passive sources are typically rich in energy over different frequency bands, with the passive sources providing usually more information in the low-frequency range. In the InterPACIFIC project, both active and passive surface wave data were collected by adopting different arrays, all of them located in the vicinity of existing boreholes, which were subsequently used for in-hole seismic measurements [41]. The active and passive array geometries and acquisition parameters utilized at Mirandola, Grenoble and Cadarache are provided in Tables 4, 6 and 8, respectively. Brief descriptions of the experimental data acquisition are provided below.

For active source data, we adopted at the three sites the linear scheme of MASW, as proposed by Park et al. [31]. The geophones are placed along a linear array and the source is in-line with them. The geophone spacing is typically a few meters or less, according to the expected V_S of the site, the required resolution and the desired investigation depth [52]. A Geode seismograph (Geometrics) and a linear array with different receiver spacing's, varying from 0.5 to 2 m according to site conditions and available space, was used for the acquisition of the datasets. Low natural frequency geophones are used to avoid phase distortions over the frequency range of interest. MASW surveys were designed and performed to acquire both Rayleigh and Love wave data. Rayleigh and Love waves data were recorded by using vertical geophones (4.5 Hz natural frequency) and Swyphone horizontal geophones (20 Hz natural frequency) [53], respectively. An 8 Kg sledgehammer was used as the seismic source, striking vertically on an iron plate for the generation of Rayleigh wave data and horizontally on an iron beam for Love wave data. The acquisition parameters were defined to allow seismic refraction data, both in terms of P- and SH- waves, to be simultaneously acquired with surface wave data [54] and, hence, it was also possible for the teams to retrieve additional information on the site.

In the case of Microtremor Array Measurements (MAM) or Ambient Vibration Array (AVA), noise source locations are unknown and 2D array layouts are used to extract the seismic wave propagation characteristics (phase velocity and direction of propagation) [55–57]. 2D arrays with 3-component sensors are adopted in this study. In addition, since the involved frequencies are quite low, the sensors are required to have high sensitivity. For sake of simplicity in setting up arrays in the field, the most common array geometries are triangular and circular [57]. The L-shape geometry is often adopted because of its simplicity and the possibility to collect data in the presence of obstacles (e.g., a building). It consists of two perpendicular lines and the geophones are typically placed along them with increasing distance from the crossing point. Also spare and irregular geometries are often implemented [58], due to practical limitations and presence of obstacles in the measuring area. Asten et al. [40] also demonstrate the use of triangular arrays where only two perpendicular lines are available such as at a road T-junction.

Within this project, passive measurements collected by linear deployment of geophones (e.g., Refraction Microtremors known also as ReMi, [59]) have not been used. As thoroughly discussed by Cox and Beekman [60] and Strobbia and Cassiani [61], this passive method is based on the assumption that ambient noise is generated by unknown sources perfectly aligned with the array or isotropically distributed around the site, but these conditions are often violated. Therefore, there is a potential for significant errors to arise when processing passive surface wave data collected with a linear array. As such, we believe 2D passive arrays should be used whenever possible and that extreme caution should be used when only utilizing linear passive arrays.

Passive data have been collected at the three sites with 15 three-component seismometers (Güralp broadband CMG-6TD with integrated digitizers), which provide a linear response between 30 s and 100 Hz. The signals were sampled at a 200 Hz sampling frequency with continuous GPS synchronization. Circular, triangular and L-shape arrays were adopted. In all the acquisitions, a sensor was placed in the reference point located close to the existing boreholes. For each circular-array acquisition, two concentric circles, centered on the reference point, were simultaneously acquired using 7 equally-spaced sensors in each circle. Circular-array diameters ranged from 5 to 405 m at Mirandola and Grenoble, and from 5 to 135 m at Cadarache, where space for larger arrays was not available. The triangular arrays were performed with 5 nested triangles, whose centroid corresponds to the reference point. The side of each triangle varies from 12.5 m to 300 m. Also a L-shape geometry dataset was collected with two perpendicular lines crossing each other in the reference point and the sensors having different distances (varying from 5 to 150 m) from this point. Even if very large arrays are not common for seismic characterization at the depth of interest in geotechnical

engineering applications, additional arrays were acquired with large geometries to investigate the possibility of deep profiling. Details on the available datasets for each site are provided in the specific sections below.

The whole set of experimental data was made available to the teams for processing and inversion. Each team was free to choose which subset of data to analyse.

2.2. Processing

The surface wave analysis typically derives the experimental dispersion curve, which is subsequently used for the inversion process. Most processing techniques are based on the transformation of the experimental gather from time-space domain to other domains, where surface-wave propagation characteristics are associated to spectral maxima (e.g., the frequency-wavenumber domain or the frequency-slowness domain). For microtremors, alternative methods are based on the spatial autocorrelation (SPAC) of the data under the assumption that the signal of interest is stochastic, stationary in time and space [26].

Rather than explicitly estimating an experimental dispersion curve, some methods adopt alternative processing procedures to invert propagation characteristics of surface waves. For example, Asten [62] makes direct use of SPAC spectra computed from smoothed coherency-frequency spectra. Forbriger [63] interprets the wavefield in terms of Fourier–Bessel expansion coefficients: surface waves appear as signals with large amplitude in the latter and the dispersion relation becomes apparent in plots of the expansion coefficients.

Alternative approaches are based on extraction of ellipticity of Rayleigh waves from single station and array processing of noise recordings (e.g. [62–65]).

A list of processing methods adopted by the different teams within this project, with the relevant literature references, is reported in Table 2.

Since active and passive data provide information regarding the surface-wave propagation over different frequency bands, it is possible to combine the branches of the dispersion curve to better constrain the final result.

Table 2
List of methods adopted for the processing of surface wave data.

Label	Method	Data	References
FK	Frequency-wavenumber transform	active	[29]
PF	Slowness-frequency transformation method	active	[30]
PS	Phase-shift transform, a special case of PF transform	active	[31]
FDBF	Frequency domain beamformer	passive	[29,68]
HFK	High resolution frequency-wave-number transform	passive	[27]
SPAC	Spatial Autocorrelation Coefficient method	passive	[26]
MSPAC	Modified SPAC	passive	[69]
3C+WD	Three component high-resolution f-k analysis and wave field decomposition	passive	[66,70]
SPAC_directFit[a]	SPAC spectra computed from smoothed coherency-frequency spectra	passive	[62]
FB[a]	Fourier-Bessel expansion coefficients	active	[63]
Ellipticity[a]	Ellipiticity of Rayleigh waves from the noise recordings	passive	[65]

[a] The experimental dispersion curve is not explicitly considered in the approach.

2.3. Inversion

The V_S profile is obtained by solving an inverse problem. The parameterization is based on the assumption of a local 1D layered model consisting of a stack of homogeneous linear elastic layers over a half-space. Each layer is characterized by its thickness (except for the half-space), density and two elastic properties: the S-wave velocity and one parameter that must be chosen between P-wave velocity and Poisson's ratio. Surface-wave dispersion strongly depends on the shear stiffness of the subsoil, less on the bulk stiffness and negligibly on density. Thus, P-wave velocity (or Poisson's ratio) and density are often assumed as a-priori known parameters, which are selected on the basis of available information on the site [71,36] or they can be retrieved from the available experimental data if opportunely acquired. For example, in the InterPACIFC project the active data were acquired to allow refraction analysis (see paragraph 2.1). This issue was deemed particularly important for allowing the teams to estimate the water table position from the refraction of P-waves, as this information is of paramount importance to set a-priori values of model parameter which are not considered as unknowns in the inversion (density and Poisson's ratio of each layer) [72]. Thus, the unknown model parameters of primary interest are the thickness and V_S of each layer. Once an initial model has been parameterized, the inversion consists in finding the final model(s) whose theoretical dispersion curve fit the experimental one.

The surface wave inverse problem is mathematically ill-posed, and it is affected by solution non-uniqueness [73]. Indeed, several profiles which give theoretical dispersion curves that fit the experimental data can be identified [74,21,75,25]. Apart from this issue of non-uniqueness, misinterpretation in the identification of dispersion curve modes (fundamental mode or higher modes) can bias the results (e.g., [76,77,15]). Non-uniqueness and errors in the identification of propagation modes are probably the main cause for doubts in the ability of surface-wave methods to recover a realistic model of the site [9]. Many authors have suggested different strategies for the inversion of surface-wave data. Some authors applied stochastic methods (e.g., [78–80,37] among the others), some adopted deterministic methods like the least-squares algorithm (e.g., [35,36,81]), while others focused on multi-mode, effective mode or joint inversion of Rayleigh and Love wave dispersion curves for better constraining the solution (e.g., [82,49,83,20,84,67,85]).

Other approaches have been proposed to retrieve S-wave velocity from surface-wave analysis that do not require an experimental dispersion curve. Forbriger [63,76] proposed a method based on a wave field transformation. In this method, Fourier–Bessel expansion coefficients are calculated for the recorded data and then these coefficients are jointly inverted with P-wave arrival times to retrieve the S- and P- wave velocity distribution of the subsoil.

The SPAC direct fitting method [86,87,62] also does not require the dispersion curve. This method relies on SPAC spectra computed from smoothed coherency-frequency spectra. The model parameters are retrieved by minimizing the error between the experimental and model coherency-frequency curves by adopting a L2 norm.

Passive data collected with 3-component receivers can also be used to obtain an estimate for the natural frequency of the site. In particular, frequency of the maxima of the Horizontal-to-Vertical Spectral Ratio (HVSR) can provide a fast and reliable interpretation in this respect [88,89]. The frequency associated to the peak of the HVSR curves can indicate the resonance of the subsoil model, and many authors related the HVSR curve to the ellipticity of Rayleigh waves [64–67,85]. Consistency between the natural frequency as estimated from the HVSR and the shear-wave velocity profile can

Table 3
List of algorithm adopted to solve the inverse problem.

Label	Algorithm	References
NA	Neighborhood Algorithm	[38]
MC	Monte Carlo method	[37,39]
GA	Genetic Algorithm	[90,34]
SA-GA	Simulated Annealing and genetic algorithm in an hybrid heuristic search method	[91]
NLS	Non-linearized least-squares algorithm	[92]
LLS_EYE	Linearized Least Square and trial and error procedure	[62,40,76]
EYE	Trial and error procedure	

be considered valuable information to improve the reliability of the model. Joint inversions of Rayleigh wave dispersion curve and HVSR are reported in the literature and provide better constrains on the V_S profile, especially for the position of major stratigraphic interfaces like depth to bedrock [49,81].

In particular, in this project several algorithms, both stochastic and deterministic, were adopted to build the V_S profile. A list of the methods and the relative references is reported in Table 3.

3. Results

The "best estimates" in terms of dispersion curves and V_S results provided by all teams are compared, taking into account the different dataset and analysis choices. It is worth mentioning that no a-priori information about subsurface layering or water table was provided to the teams.

Below, a brief description of the geology at each site is provided together with the main results and some relevant comparisons. The comparisons of the results take into account: the seismic dataset that was processed; the kind of surface wave (Rayleigh and/or Love, indicated as R and L, respectively) and the propagation mode (indicated as 0 for fundamental mode and increasing number for higher modes, and E for effective/apparent mode); the method that was adopted to retrieve the dispersion curve (according to Table 2); the search/optimization method adopted in the inversion (according to Table 3); and if additional information that can be retrieved by the data (e.g. water table, ellepticity, etc.) was introduced.

We investigate in this paper also the relationship between the retrieved wavelength (λ) and the estimated V_S profile. The λ band provides information on the investigation depth range. In particular, the investigated depth is often assumed roughly equal to $\lambda/3$–$\lambda/2$ when the fundamental mode of Rayleigh wave is considered dominant in the inversion [93]. Good practice when interpreting dispersion-curve data recommends the maximum investigated depth (d_{max}) should not be greater than approximately half of the maximum retrieved wavelength (i.e., $d_{max} < \lambda_{max}/2$), as dictated by the necessity of sufficient information to constrain the solution. A more conservative approach, and possibly better practice, would be to limit the max depth of the V_s profile to $\lambda_{max}/3$. Conversely, at a very shallow depths, the minimum thickness of the first layer (h_{min}) that can be defined should ideally not be less than 1/3 the minimum retrieved wavelength (i.e., $h_{min} > \lambda_{min}/3$), if only the fundamental mode of Rayleigh waves is used in the inversion. A more conservative approach, and possibly better practice, would be $h_{min} > \lambda_{min}/2$.

The use of higher modes of Rayleigh and Love waves and Rayleigh wave ellipticity may help in mitigating these limitations. In the presence of a large impedance contrast, the maximum investigation depth can be significantly poor, if no additional constraint is used for the inversion, such as the HVSR polarization function. Where dispersion curve is supplemented by interpretation of HVSR data, then the frequencies of maxima in the HVSR may allow use of longer wavelengths and estimation of the V_S profile to depths greater than those defined by the rules above (see examples in [40,92]).

Each team indicated the investigated depth with the submission of its own results. This is a subjective choice of each analyst on the basis of the available information, inversion strategies, previous experience and so on.

The results provided by the teams were compared also in terms of $V_{S,Z}$ i.e. time-average shear wave velocity in the topmost z meters according to:

$$V_{S,z} = \frac{z}{\sum_{i=1}^{N} \frac{H_i}{V_{S,i}}} \quad (1)$$

in which N is the number of layers used for the discretization of the model from the surface to z and H_i and $V_{S,i}$ are the thickness and shear wave velocity for each layer i, respectively. The value for $z=30$ m is the $V_{S,30}$. Moreover $V_{S,Z}$ can be used to compare the expected site amplification for two different shear wave velocity profiles [95].

In addition, the variability of the results is evaluated through the estimation of the Coefficient of Variation (CoV) of the phase velocity as function of depth. This parameter is computed as the ratio between standard deviation over the mean value of the population of results.

3.1. Mirandola

The geology of the Mirandola site (MIR) consists of alluvial deposits with sandy horizons and silty-clayey layers, overlying a stiffer layer of marine and transitional rock-like deposits of lower-middle Pleistocene age at a depth between 50 and 150 m from the ground. The site is flat and it is rather quiet, being at the border of a residential area, without noisy facilities. The seismic datasets, acquired according to the arrays showed in Fig. 2, are detailed in Table 4.

All the teams analysed the fundamental mode of Rayleigh wave, some teams also analysed the higher modes or effective mode, while others included Love wave analysis (Table 5). Another popular choice was the combination of the information retrieved from both active and passive seismic datasets, as reported in Table 5. The lowest mode Rayleigh wave dispersion data obtained by each team (presumed to be either fundamental mode or an effective mode) are compared in Fig. 3 (top). Most analysts obtained Rayleigh wave dispersion estimates within a frequency band of approximately 1–20 Hz (Fig. 4). The dispersion estimates within this bandwidth generally agree very well, being characterized by a coefficient of variation (CoV) typically between 5% and 10% (Fig. 3, bottom). The CoV values begin to climb rapidly at higher and lower frequencies. For the high-frequency band, this observation is likely associated to lateral variability in the very shallow part of the deposit, whereas in the low-frequency band the estimates are approaching the limit of resolvable frequency accounting for array geometry and data quality. CoV values were not estimated for frequencies with results from less than 5 analysts.

The frequency band (Fig. 4) is wider for those who combined active and passive data, while it is slightly narrower for those who relied exclusively on either active or passive data. The frequency band retrieved with passive data is centered at lower values.

Fig. 5 (top 500 m) and Fig. 6 (top 150 m) show the V_S profiles and the time-averaged V_S profiles ($V_{S,Z}$) obtained by the teams by adopting the search/optimization method reported in Table 5. The CoV values and number of analysts for a given depth are also provided. Considering the first 90 m, which is a significant depth

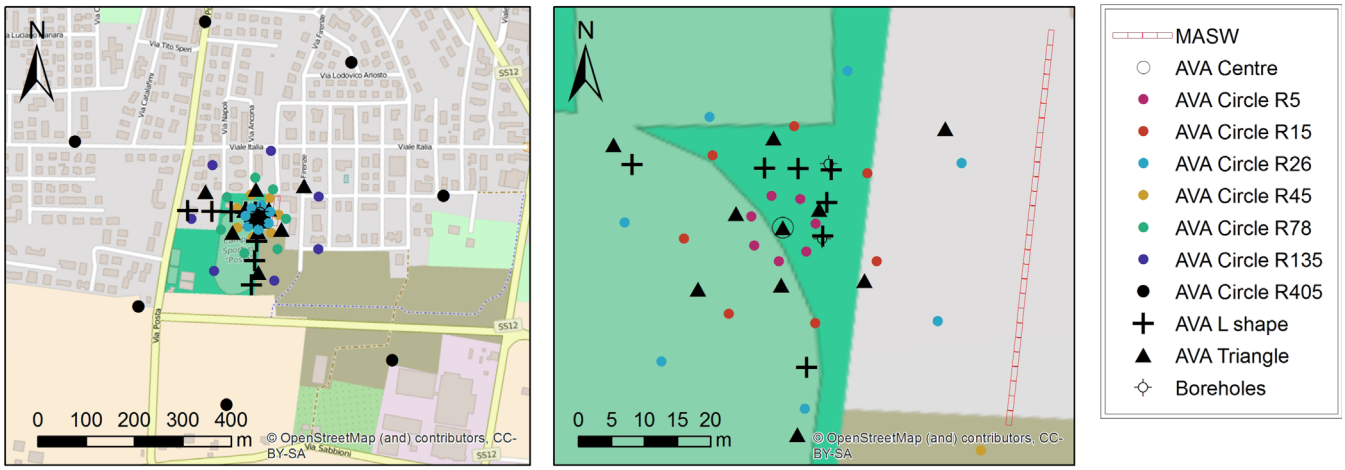

Fig. 2. Mirandola: maps of the arrays. (Left) whole area interested by the acquisition. (Right) close-up view of the area. The largest triangular array is not shown.

Table 4
Mirandola: datasets. T= time window, ΔT=time sampling.

label	Dataset	Num. channels	Time sampling	Space sampling
AV1	Active (vertical)	48	T=2 s, ΔT= 0.25 ms	Receiver spacing=1 m
AV2	Active (vertical)	48	T=2 s, ΔT= 0.25 ms	Receiver spacing=2 m
AH	Active (horizontal)	24	T=2 s, ΔT= 0.25 ms	Receiver spacing=2 m
PC1	Passive circular	15	T=01:00:00 ΔT= 5 ms	Radii=5 and 15 m
PC2	Passive circular	15	T=01:15:00 ΔT= 5 ms	Radii=15 and 45 m
PC3	Passive circular	15	T=01:13:00 ΔT= 5 ms	Radii=45 and 135 m
PC4	Passive circular	15	T=01:58:30 ΔT= 5 ms	Radii=135 and 405 m
PC5	Passive circular	15	T=01:20:00 ΔT= 5 ms	Radii=26 and 78 m
PT	Passive triangular	16	T=01:29:00 ΔT= 5 ms	Sides=12.5, 25, 50, 100, and 200 m
PT2	Passive large triangular	10	T=03:24:30 ΔT= 5 ms	Sides=4000, 2000, 1000 m
PL	Passive L-shape	13	T=00:59:30 ΔT= 5 ms	Distances=5, 10, 30, 60, 100, and 150 m

for most site characterization projects, the agreement is very good, with CoV values typically around 0.1. Considering that no a-priori information was available to the teams to further constrain the inversion, these results are quite remarkable. However, the agreement between analysts is not very good at depths greater than about 100 m, where CoV values based on the standard layered V_S profiles consistently exceed 0.5. Interestingly, the CoV values based on the smooth $V_{S,Z}$ profiles remain less than 0.2 clear down to 500 m. In the close-up view figure (Fig. 6a), it is possible to notice that the results are in good agreement with each other until roughly between 85 and 140 m depth, where a strong interface is expected, but this feature was not uniquely identified by all teams. This is the reason for the high value of CoV in such depth range (Fig. 6c). Deeper than this interface, the results show mainly two trends: one at 700 m/s and a second one at 1250 m/s.

Fig. 7 left shows the relationship between λ_{min} and the thickness of the first layer while Fig. 7 right shows the relationship between λ_{max} and maximum investigated depth. Most of the results are in agreement with the aforementioned good-practice recommendations and very few points fall in the "not-recommended" area. It is important to highlight that here we analysed only the wavelength of the Rayleigh fundamental mode and those analysts who violated the criteria have supplied information in depth with other kind of information (i.e., HVSR frequency, Rayleigh wave ellipticity).

3.2. Grenoble

Grenoble site (GRE) was chosen as representative of a stiff-soil class since it is characterized by recent alluvial materials for few ten meters from the surface overlaying a Quaternary clayley-marly deposit. A Mesozoic bedrock is expected at several hundred meters depth, namely between 500 and 800 m depth [43]. In this site no topographic variability is observed. The site is in a highly industrialized area of Grenoble (France). In addition, two highways with high traffic and two rivers (Isere and Drac) are in the vicinity of the site. In this site a low-velocity layer, roughly 10-m thick, is expected at around 25 m depth but such information was not provided to the teams.

Here the datasets reported in Table 6 and according to the array showed in Fig. 8, were acquired and the teams processed the data adopting the strategies reported in Table 7.

Fig. 9 (top) shows the lowest mode (presumed to be either fundamental mode or an effective mode) of Rayleigh wave dispersion data obtained by each team. Most analysts obtained Rayleigh wave dispersion estimates between frequencies of approximately 0.7–50 Hz. The dispersion estimates within this bandwidth agree very well, being characterized by a coefficient of variation (CoV) typically less than 5% (Fig. 9, bottom). CoV values were not estimated for frequencies with results from less than 5 analysts. The CoV values begin to climb rapidly at high frequencies, likely because of lateral variation. Indeed some near-surface lateral variability was observed at the site when processing the active source data from the two different close-by linear arrays (center-to-center distance equal to about 100 m). This is consistent with the local geology characterized by recent alluvial deposits with coarse materials in the top meters.

We also note that all teams provided dispersion curves that were able to identify an inverse trend (localized low/flat phase velocity zone) in the 2–10 Hz frequency range (Fig. 9, top). This

Table 5
Mirandola: processing and inversion strategy for each team.

ID	Team	dataset	Surface wave mode	Additional information	Dispersion analysis processing	Inversion algorithm	Software
1	MU	PC1, PC3, PT, PT2	RE	HVSR	SPAC_directFit	LLS_EYE	Mmspacfit
2	CE	PT	R0	HVSR	SPAC+FK	NA	Geopsy
3	IST1	PC1, PC2, PC3, PC4, PC5	R0 R1, L0	Ellipticity	FK	NA	Geopsy
4	UT	AV1, AV2, AH, PC1, PC2, PC3, PC4, PC5, PT, PL	R0, R1, L0		SPAC+FDBF	NA	Geopsy
5	INGV	AV1, AV2, AH, PC1, PC2, PC3, PC4, PC5, PT, PT2, PL	R0, L0, L1	HVSR	FK	NA	Geopsy
6	BFO	AV1, AV2, AH	R0, R1, R2		FB	LLS_EYE	Germlin (In-house)
7	Geom	AV2, PC1, PC5, PT2	RE	HVSR	PS	GA	Seisimager
8	IST2	PC1, PC2, PC3, PC4, PC5	R0	HVSR	FK	NA	Geopsy
9	KU	PC1, PC2, PC4, PC5, PT, PT2	R0		SPAC	EYE	In-house
10	TT	PT	R0		SPAC	SA-GA	In-house
11	GV	AV1, AV2, PC1, PC2, PC3, PC4, PC5	R0	Water table (refraction analysis)	SPAC+PS	NLS	Seisimager; WinSASW
12	SED	PC1, PC2, PC3, PC4	R0, R1, R3, R4, L0, L1	Ellipticity	3C+WD	NA	In-house; Dinver
13	PU		R0		SPAC	NA	Geopsy
14	PT	AV1, AV2, PC3, PC4	R0		FK+FDBF	MC	in-house

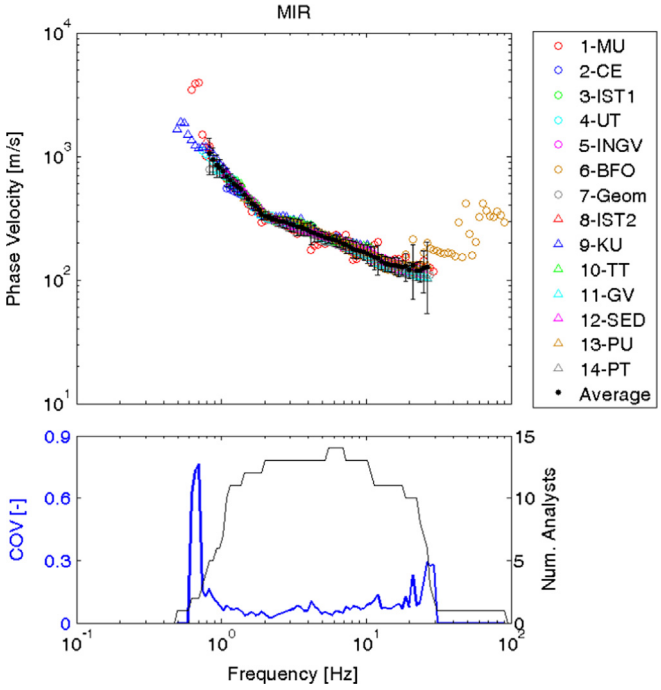

Fig. 3. Mirandola: (top) fundamental mode of Rayleigh wave dispersion curves. (bottom) Number of analyst and CoV.

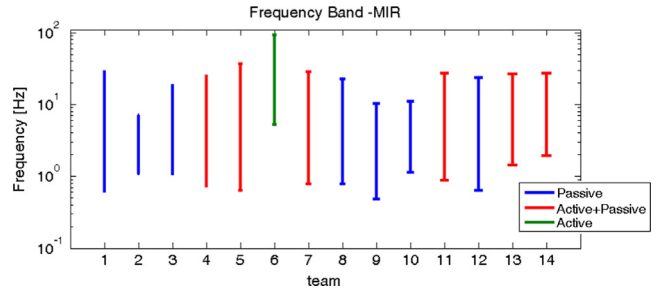

Fig. 4. Mirandola: frequency band associated with the retrieved dispersive curve or earth model interpretation.

inverse trend in phase velocity is characteristic of a low-velocity layer beneath a stiffer near-surface layer(s). This information was not communicated to participants, but most analysts recognized the appropriateness of including a low-velocity layer to accurately model the site.

The choice of analysing both active and passive data was the most popular at this site, while a few teams decided for analysing only the passive data and none analysed only the active data (Table 7). The analysis of both active and passive data allows for a wider frequency band (Fig. 10) than the ones of those teams that analysed just passive data, focusing more on the lower frequency and hence neglecting the higher ones. As mentioned above, the ability to retrieve high frequency/short wavelength dispersion data is important for resolving near-surface layering which may be relevant for geotechnical engineering purposes.

Fig. 11 (top 800 m) and Fig. 12 (top 150 m) show the V_S (Figs. 11a and 12a) and the $V_{S,Z}$ (Figs. 11b and 12b) profiles obtained by the teams by adopting the inversion method reported in Table 7. The CoV values and number of analysts for a given depth are also provided (Figs. 11 and 12, c and d panels, respectively). Considering the first 130 m, which is a significant depth for most site characterization projects, the agreement is once again quite good, with CoV values typically around 0.15 or less. Furthermore, the slightly higher CoV values over the top 20 m are primarily driven by a single V_s profile that is significantly different than the others. The agreement between analysts is lost at depths greater than about 200 m, where CoV values based on the standard layered V_s profiles consistently exceed 0.4. Interestingly, the CoV values based on the smooth $V_{S,Z}$ profiles rarely exceed 0.1 clear down to 800 m. In the close-up view figure (Fig. 12a), it is possible to notice that some analysts (approximately 50%) tried to resolve a low-velocity layer somewhere between 20–50 m below the surface. While a low-velocity layer does indeed exist in the soil profile (as found by invasive tests, see [41]), the analysts were not able to uniquely resolve its depth and thickness.

The relationships between the minimum/maximum experimental wavelength and the thickness of the first layer/maximum depth are reported in Fig. 13. As observed in Mirandola, some results fall in the "not-recommended" area for the maximum depth (Fig. 13, right). These results supplied the lack of low frequency of the fundamental mode with other addition information as HVSR and ellipticity. As far as the definition of the thickness of the first layer is concerned (Fig. 13, left), the 25% of the teams retrieved a thickness much smaller than the minimum experimental wavelength, resulting in lack of constraint on parameters for the first layer.

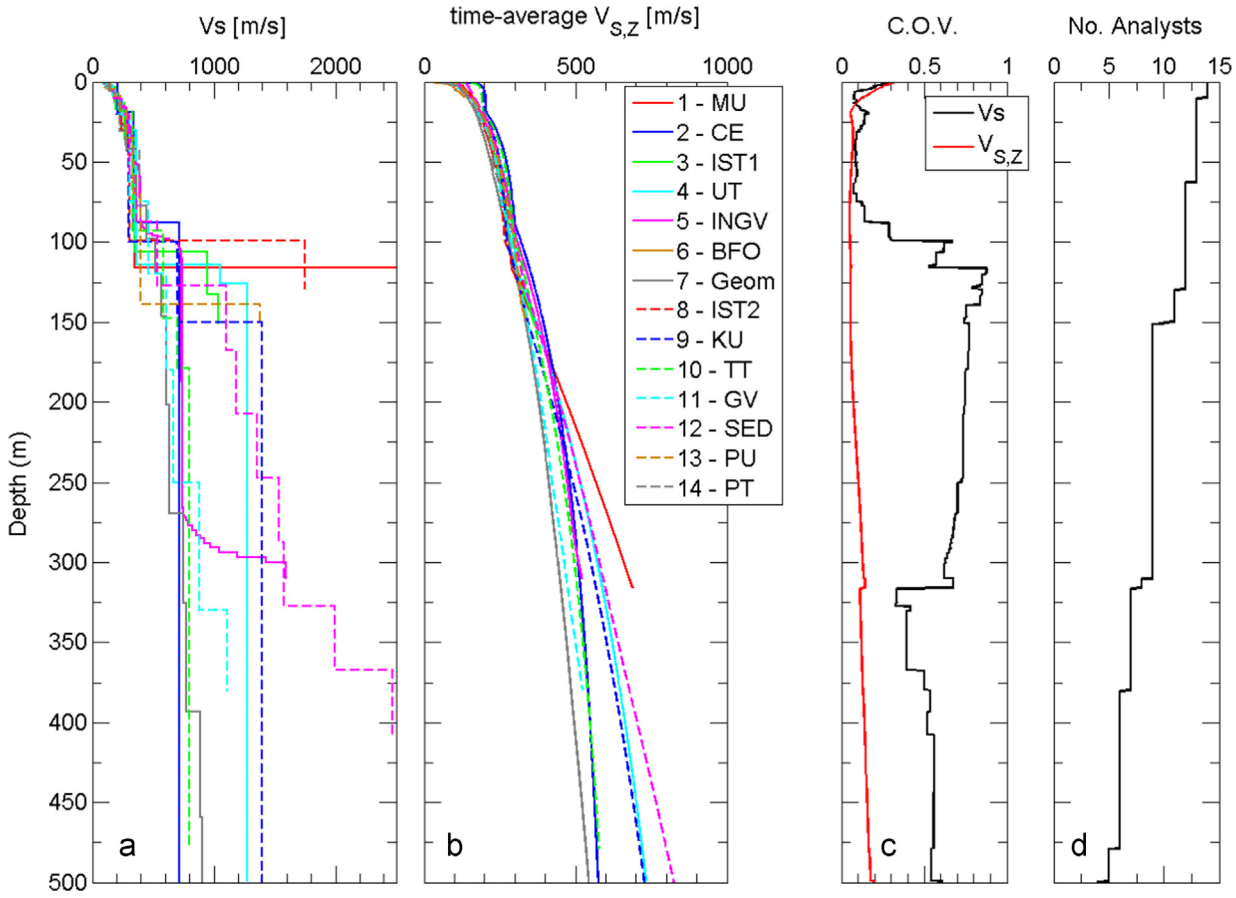

Fig. 5. Mirandola: (a) shear wave velocity (V_S) profiles, (b) time-averaged $V_{S,Z}$ profiles, (c) CoV(V_S) and CoV($V_{S,Z}$) values, and (d) number of profiles.

3.3. Cadarache

The Cadarache site (CAD) is in the area of the CEA (Commissariat à l'Énergie Atomique et aux Énergies Alternatives) Cadarache research center in the township of Saint-Paul-lez-Durance, in the south-east of France. It is located on a flat zone at the top of a small hill. A Cretaceous limestone is outcropping in the surroundings of the test site. Despite being in an industrial area, the density of facilities around the site is quite low.

The datasets reported in Table 8 were acquired according to the arrays showed in Fig. 14, and the teams processed the data adopting the strategies reported in Table 9.

The lowest mode Rayleigh wave dispersion data obtained by each team (presumed to be either fundamental mode or an effective mode) are shown in Fig. 15 (top). Many analysts obtained Rayleigh wave dispersion estimates between frequencies of approximately 0.7–100 Hz (Fig. 15, bottom). However, the dispersion estimates only agree well at frequencies less than approximately 30 Hz, as characterized by CoV values less than about 10%. The CoV values at frequencies greater than 30 Hz climb rapidly, reaching 30%. It is clear that the high frequency/short wavelength data was of poor quality. This was most certainly the result of lateral variability/local fracturing and weathering patterns in the near-surface rock mass. While CoV values were not estimated for frequencies with results from less than 5 analysts, the low frequency dispersion estimates are still in remarkable agreement from 0.3–0.7 Hz. This flattening of the dispersion trend at low frequencies is rarely observed, but allows the analyst a much more confident estimate of the half-space/basement rock velocity (i.e., approximately 2500 m/s).

Some teams were able to identify higher modes, while other were not. Also in this site, the choice of analysing both active and passive data was the most popular, few teams used only passive data and only one team (14-PT) decided to analyse only active data. The analysis of both active and passive data allows for a wider frequency band (Fig. 16), which is beneficial in terms of both near-surface resolution and maximum depth of investigation.

Fig. 17 (top 500 m) and Fig. 18 (top 100 m) show the V_S (a panels) and the $V_{S,Z}$ profiles (b panels) obtained by the teams by adopting the search/optimization method reported in Table 9. The CoV values and number of analysts for a given depth are also provided (c and d panels, respectively). As far as the CoV of V_S is concerned, these values over the top 20 m are considerably larger, while they ultimately stabilize at a value of 0.1 or less for most of the 500 m profile. Indeed, the CoV values near the surface are as high as 0.5. This is a direct consequence of the significant uncertainty in the high-frequency dispersion data shown in Fig. 15, which was most likely the result of lateral variability/local fracturing and weathering patterns in the near-surface rock mass. Conversely from the other two sites, it is interesting to observe that the CoV of $V_{S,Z}$ has the same trend of V_S. Therefore, teams were not able to identify a unique depth to the shallow, hard bedrock (i.e., $V_S > 2000$ m/s).

As far as the analysis of the retrieved wavelength is concerned (Fig. 19), similar comments of the ones reported for the other two sites can be drawn. Most of the teams defined the V_S model until a depth consistent with the most restrictive criterion with respect to maximum wavelength (Fig. 19, right). Also the thickness of the first layer is typically consistent with good practice recommendations,

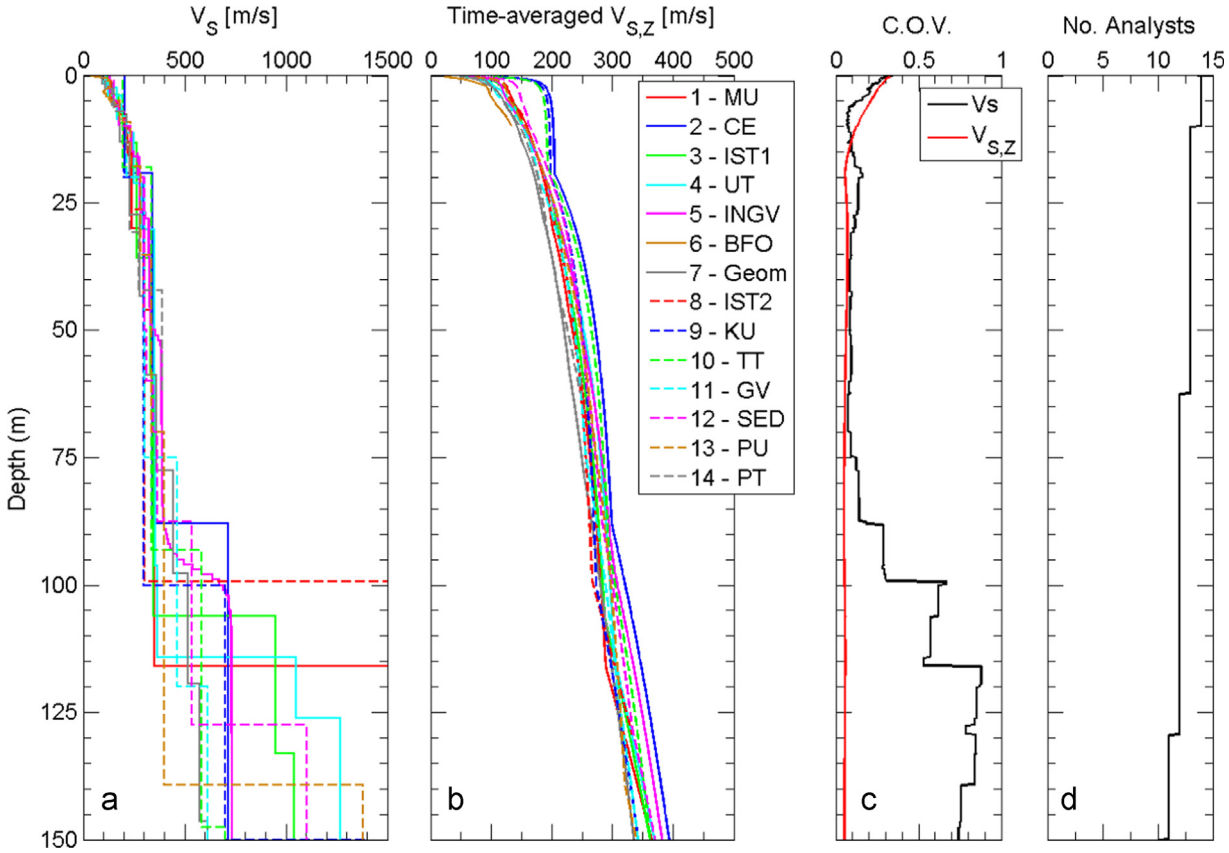

Fig. 6. Mirandola: close-up view of the top 150 m of Fig. 5.

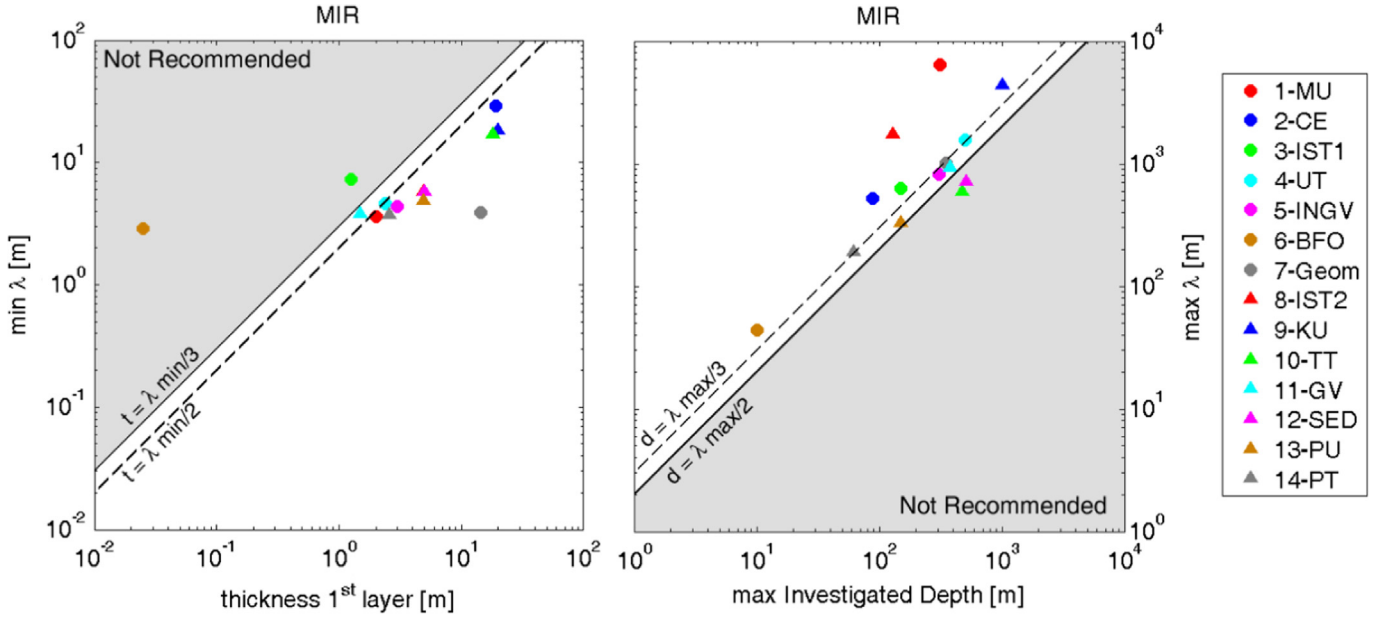

Fig. 7. Mirandola: (left) thickness of first layer as function of the minimum retrieved wavelength. (Right) maximum investigated depth as function of the maximum retrieved wavelength. In gray the "not-recommended" part of the domain.

even if some teams are slightly out of the recommended threshold (Fig. 19, left).

3.4. Variability of the results

The variability of best estimates observed among participants is most probably caused by one (or many) of the following reasons:

- difference in interpreted experimental data (frequency range, Rayleigh/Love waves, fundamental/higher modes),
- non-uniqueness of the inversion that can lead to several different best estimates of V_S (here only one of the best estimates for each participant is taken into account in the comparison),
- different choices for the parameterization of the inversion (i.e., number of layers),

Table 6
Grenoble: datasets. T= time window, ΔT=time sampling.

Label	Dataset	Num. channels	Time sampling	Space sampling
AV1	Active (vertical)	48	T=2 s, ΔT= 0.25 ms	Receiver spacing=1 m
AV2	Active (vertical)	48	T=2 s, ΔT= 0.25 ms	Receiver spacing=1.5 m
PC1	Passive Circular	15	T=01:37:00 ΔT= 5 ms	Radii=5 and 15 m
PC2	Passive Circular	15	T=01:01:00 ΔT= 5 ms	Radii=15 and 45 m
PC3	Passive Circular	15	T=01:35:30 ΔT= 5 ms	Radii=45 and 135 m
PC4	Passive Circular	15	T=01:21:30 ΔT= 5 ms	Radii=26 and 78 m
PC5	Passive Circular	16	T=02:00:00 ΔT= 5 ms	Radii=78 and 405 m
PT	Passive Triangular	16	T=01:55:30 ΔT= 5 ms	Side=18.75, 37.5, 75, 150 and 300 m
PL	Passive L_Shape	13	T=01:07:00 ΔT= 5 ms	Distances=5, 10, 30, 60, 100, and 150 m

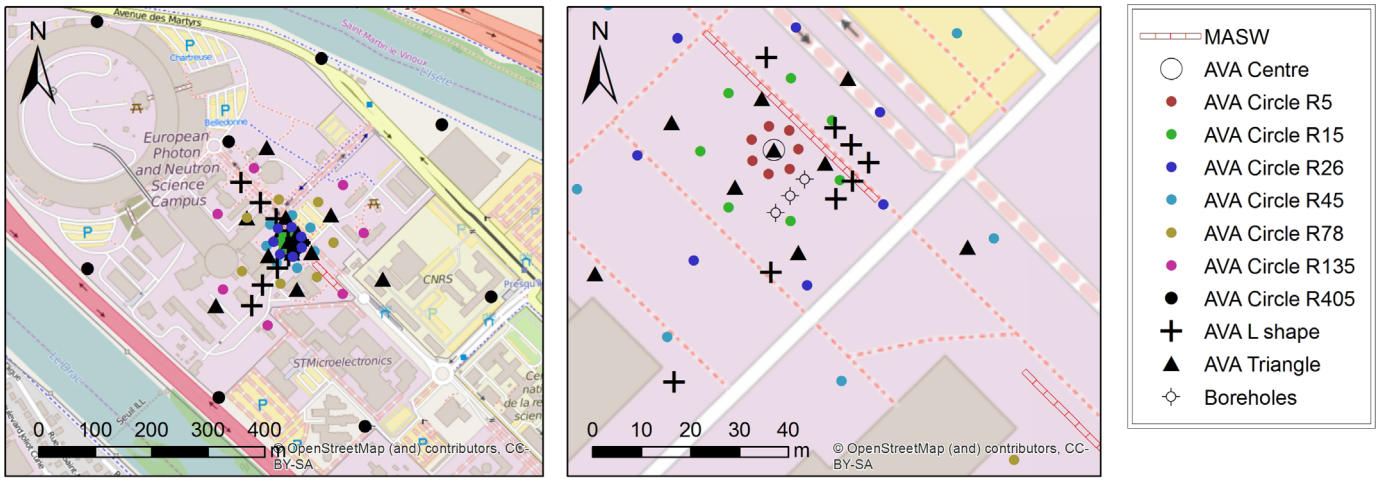

Fig. 8. Grenoble: map of the arrays. (Left) whole area interested by the acquisition. (Right) close-up view of the area.

- use of extra information/data (water table depth, HVSR resonance frequency, Fourier amplitude spectra, ellipticity, etc …)

In order to quantify the variability of the obtained results in three different subsoil conditions, we compared the CoV of V_S obtained in all the three sites as shown in Fig. 20. For all the three sites, the CoV is higher in those parts of the models in which it was difficult to recognize some specific features (e.g., interfaces between layers). In the shallow part, Cadarache shows a greater value of the ratio than the others sites but then the value settles around 0.06 and remains constant. This observation reflects the variability that we observed in the results related to the identification of the shallow zone in which there is a transition between altered and competent rock. This variability is also likely associated to possible lateral variations in the alteration zone and to the use of different subset of available experimental data to estimate the dispersion curve. In Grenoble, the velocity ratio remains on average constant for the whole investigated depth, with some local differences associated to the transition between different materials. In Mirandola the CoV assumes a high value (about 0.3) close to the ground surface, reflecting the lack of resolution due to the adopted parameterization and/or to the limited frequency band of the dispersion curve for some teams. Low values of the velocity ratio are obtained for intermediate depths, with a local increase at around 25 m where a stratigraphic interface is located according to evidences in borehole logs at the site. The variability then increases abruptly when approaching to the bedrock position which, according to borehole logs (see the companion paper [41]), is to be found around 110 m depth.

Some teams used information from the HVSR to check or constrain the bedrock position. Fig. 21 reports a comparison between their best V_S estimates and the ones by teams which did not account for HVSR for Mirandola site. Apparently, a better definition of the bedrock position at approximately 110 m is achieved when HVSR information is taken into account, even if this advantage is not reflected in a reduced variability on V_S values of the bedrock.

As the $V_{S,30}$ is adopted as a reference parameter for soil classification in building codes and for the development of empirical Ground Motion Prediction Equations (GMPEs), it is relevant to assess its observed variability in the ensemble of available results for the three sites. No specific request to estimate $V_{S,30}$ was posed to the participants, hence their analyses might not have been tailored to get an accurate estimate (e.g., by paying special attention to the resolution in the zone close to ground surface).

In addition to the formal evaluation for any given V_S profile according to Eq. (1) for z=30 m, $V_{S,30}$ can be also estimated directly from the dispersion curve as proposed by Brown et al. [96] according to the equation:

$$V_{S,30} = 1.076 \bullet V_{R,36} \quad (2)$$

in which $V_{R,36}$ is the experimental phase velocity of Rayleigh wave fundamental mode for λ=36 m.

In Table 10 we compare the $V_{S,30}$ computed from the V_S profiles (Inv) according to Eq. (1) for z=30, with the $V_{S,30}$ computed directly from the dispersion curves (dc) according to Eq. (2). Such results are reported in terms of mean value, standard deviation (std), coefficient of variation (CoV). Apparently, the results at

Table 7
Grenoble: processing and inversion strategy for each team.

ID	Team	dataset	Surface wave mode	Additional information	Dispersion curve processing	Inversion algorithm	Software
1	MU	PC4, PT	RE	HVSR	SPAC_directFit	LLS_EYE	Mmspacfit
2	CE	PC5	R0	HVSR	SPAC+FK	NA	Geopsy
3	IST1	AV2, PC1, PC2, PC3, PC4	R0	HVSR	SPAC+FK	NA	Geopsy
4	UT	AV1, AV2, PC1, PC2, PC3, PC4, PC5, PT, PL	R0, R1		SPAC+FDBF	NA	Geopsy
5	INGV	AV1, AV2, PC1, PC2, PC3, PC4, PC5, PT, PL	R0	HVSR	FK	NA	Geopsy
7	Geom	AV2, PC2, PC4, PC5, PT	RE	HVSR	SPAC+PS	GA	Seisimager
8	IST2	AV1, AV2, PC1, PC2, PC3, PC4, PC5	R0	HVSR	SPAC+FK	NA	Geopsy
9	KU	PC1, PC2, PC3, PC4, PC5, PT	R0		SPAC	EYE	In-house
10	TT	PT	R0		SPAC	SA-GA	In-house
11	GV	AV2, PC1, PC2, PC3, PC4, PC5	R0		SPAC+PS	NLS	Seisimager; WinSASW
12	SED	PC1, PC2, PC3, PC4, PC5	R0, R1, L0, L1, L2	ellipticity	3 C+WD	NA	In-house; Dinver
14	PT	AV2, PC2	R0		FK+FDBF	MC	In-house

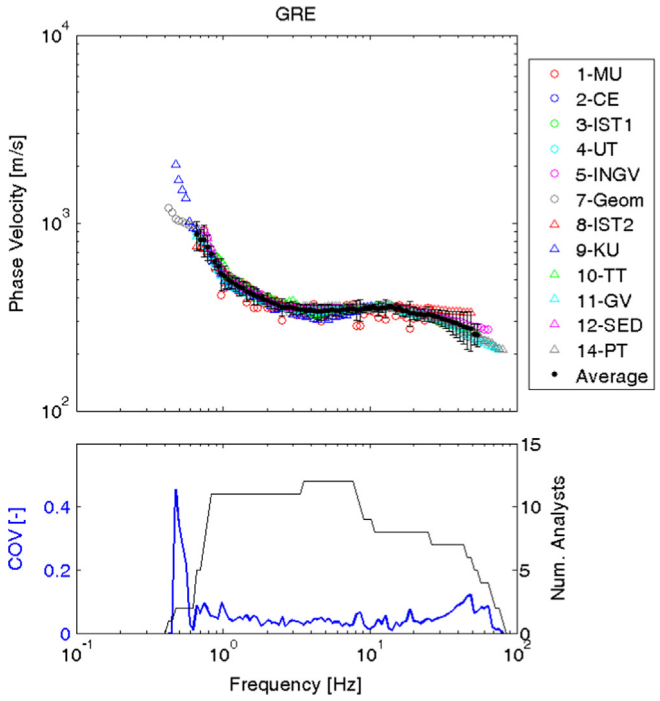

Fig. 9. Grenoble: (top) fundamental mode of Rayleigh wave dispersion curves. (bottom) number of analysts and COV.

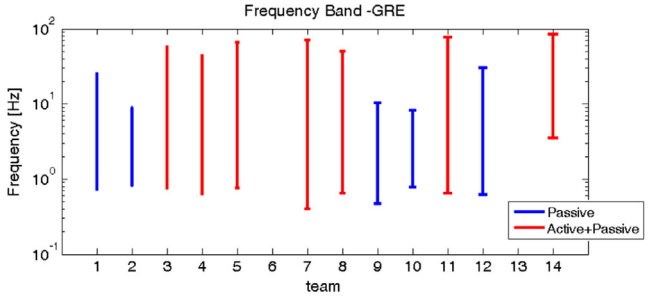

Fig. 10. Grenoble: frequency band associated with the retrieved dispersive curve or earth model interpretation.

Cadarache show a larger variability, but at this site the population of results is limited (no more than 9 samples). Thus, we report also the ratio between the maximum and the minimum values of each population of results. For the three sites, and hence for three different subsoil conditions, almost the same variability of the results is observed. It is also interesting to observe that the $V_{S,30}$ computed directly from the dispersion curve is very close to the one computed from the inverted V_S profile and it shows a very low variability as we observed in the dispersion curves.

4. Discussion

Most of the teams, in all the three sites, analysed the fundamental Rayleigh mode and the most popular processing methods were SPAC-based (preferred for the passive data) and f-k analysis. Despite the different strategies, the dispersion curves are in very good agreement with each other in all the three sites, which means in three very different subsoil conditions. This observation confirms the robustness and precision in the estimate of the experimental dispersion curve, which was observed also in previous comparative analyses (e.g., [15,16]). Higher values of the coefficient of variation of the dispersion curves at high frequencies reflect lateral variability that is often observed in different geological environment in the shallow layers.

The frequency band retrieved by each group differs from each other and it depends on the seismic dataset they analysed. As one expects, the active data provide more information at high frequency and hence they are more suitable for the characterization of the very shallow layer, while the passive ones are more at low frequency and hence better for deep characterization. However, the combination of the information from both active and passive data allows retrieving the dispersion curve over a wider frequency band, providing a better constrain to the model both in the shallow and in the deep portions. Also the information about the retrieved wavelength gives us a rough idea of the consistency of the final model. If only the Rayleigh wave fundamental mode is analysed, the maximum wavelength provides us the maximum depth to which consider reliable the final model while the minimum wavelength the maximum resolution able to retrieve. The near-surface layer thickness should also comply with typical site conditions. Indeed, thick, uniform near-surface layers rarely exist in nature. A greater resolution of the shallow part of the model is need for geotechnical engineering purposes (e.g., site response or soil liquefaction evaluation). Such resolution is achieved usually when active data are analysed. When using only passive data, usually a lack of high frequency information is observed, thus the use of a large surface layer (unrealistic but representative of average conditions) is a necessity. In case of lack of direct constraints, introducing too small layers would only bring to biased results. Most teams followed the typical

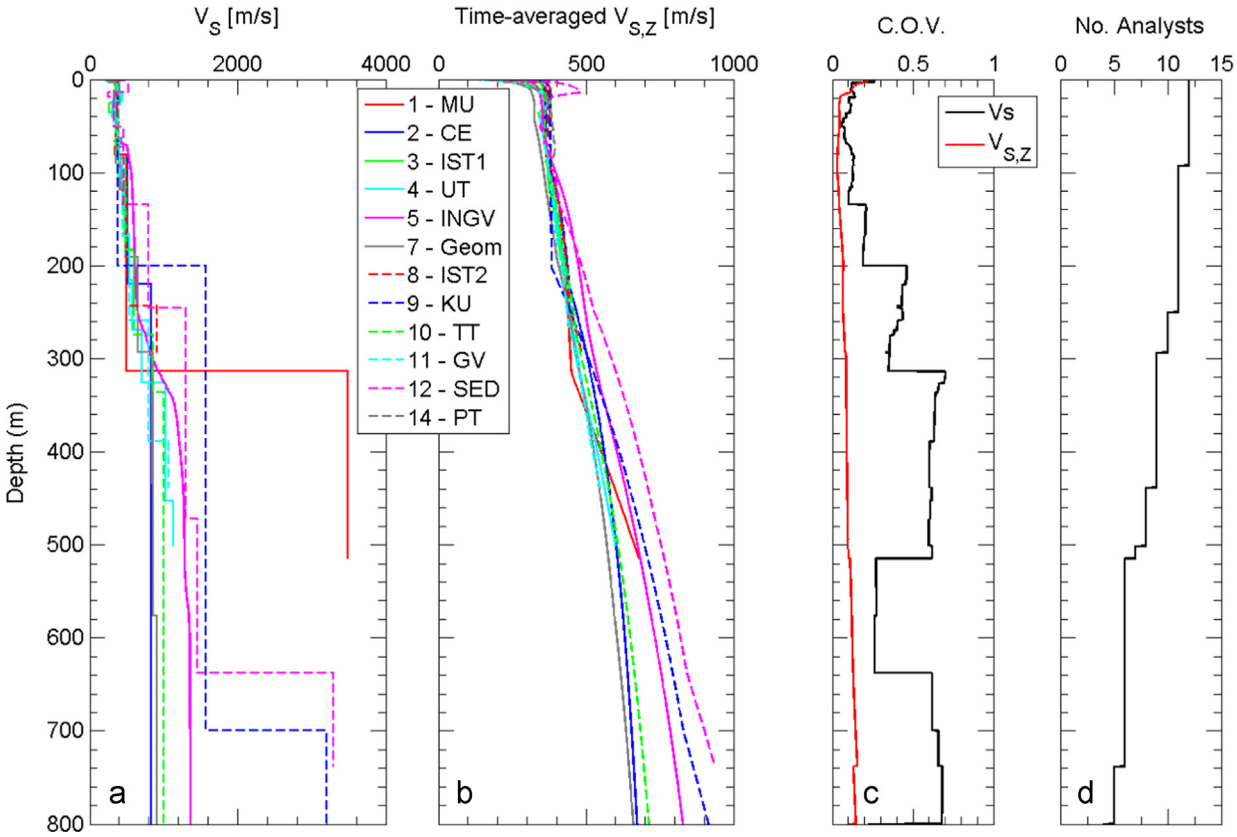

Fig. 11. Grenoble: (a) shear wave velocity profiles, (b) time-averaged V_S ($V_{S,Z}$) profiles, (c) CoV(Vs) and CoV($V_{S,Z}$) values, and (d) number of profiles.

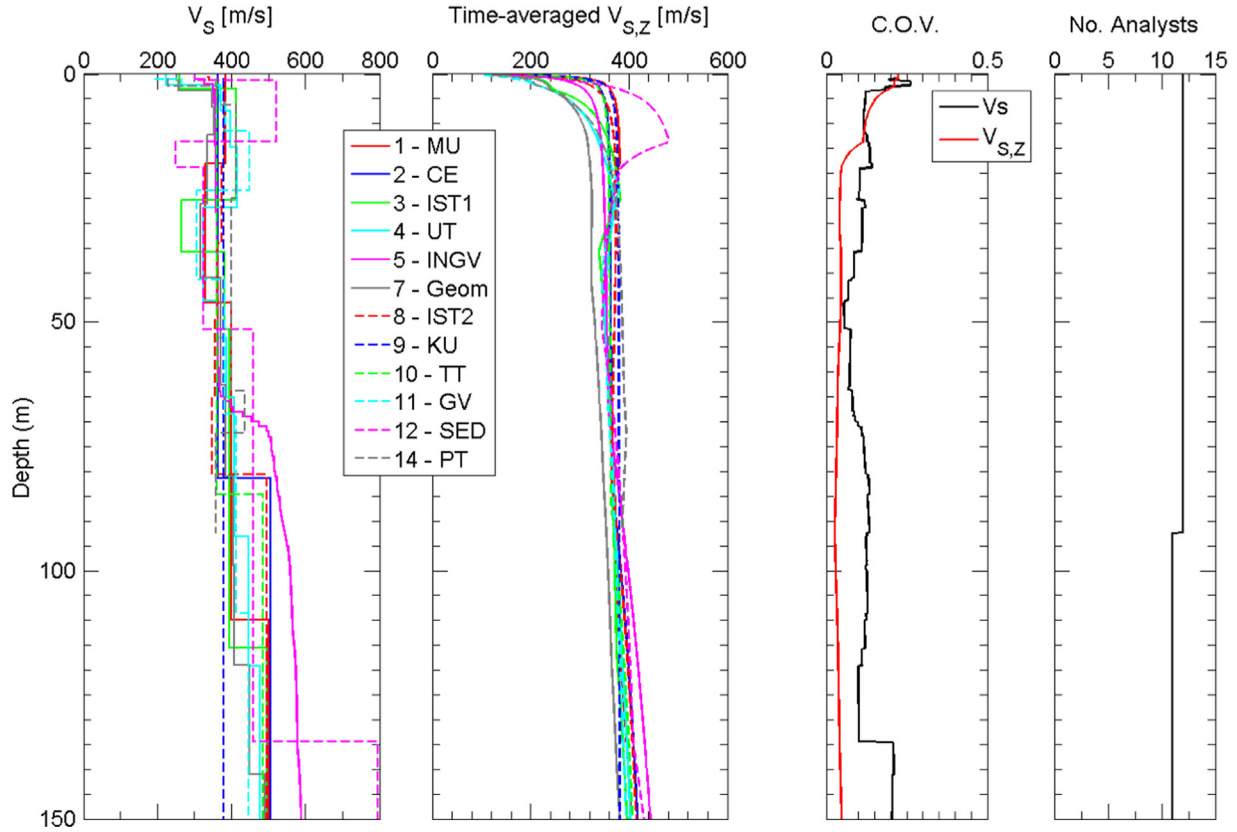

Fig. 12. Grenoble: close-up view of the topmost 150 m of Fig. 11.

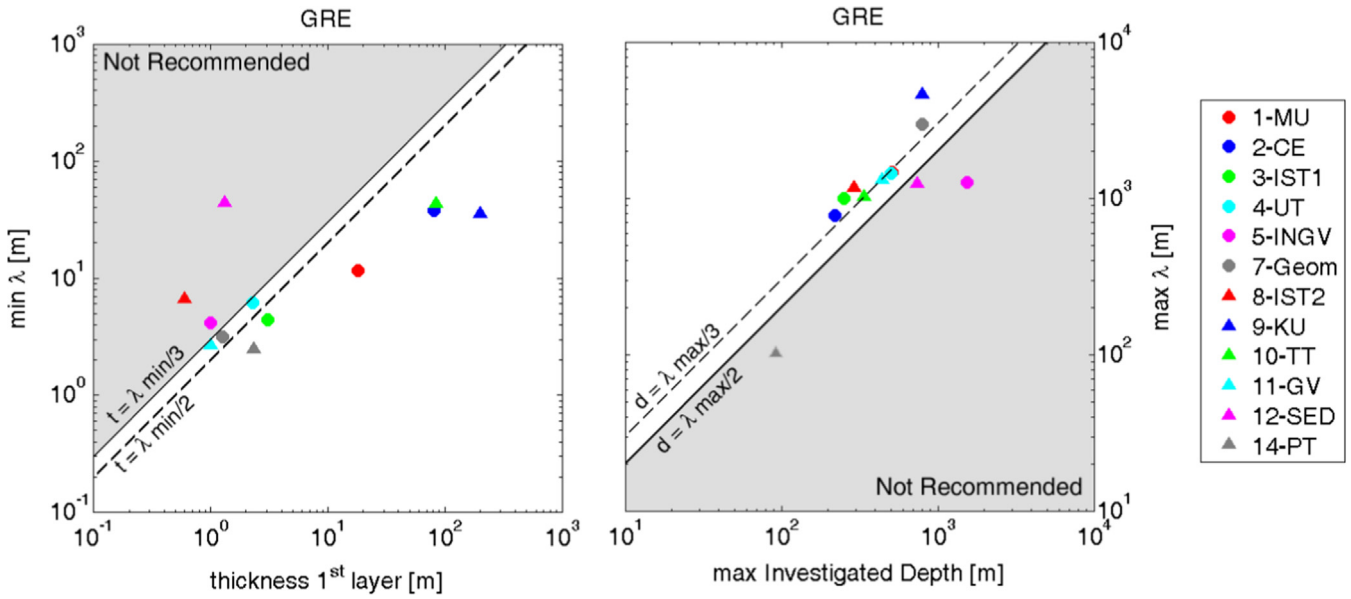

Fig. 13. Grenoble: (left) thickness of first layer as function of the minimum retrieved wavelength. (Right) maximum investigated depth as function of the maximum retrieved wavelength. In gray the "not-recommended" part of the domain.

Table 8
Cadarache: datasets. T= time window, ΔT=time sampling.

Label	Dataset	Num. channels	Time sampling	Space sampling
AV1	Active (vertical)	48	T=2 s, ΔT=1 ms	Receiver spacing=0.5 m
AV2	Active (vertical)	48	T=2 s, ΔT=1 ms	Receiver spacing=1 m
AH1	Active (horizontal)	24	T=2 s, ΔT=0.25 ms	Receiver spacing=1 m
AH2	Active (horizontal)	24	T=2 s, ΔT=0.25 ms	Receiver spacing=2 m
PC1	Passive Circular	15	T=00:54:30 ΔT=5 ms	Radii=5 and 15 m
PC2	Passive Circular	15	T=00:43:30 ΔT=5 ms	Radii=15 and 45 m
PC3	Passive Circular	15	T=01:06:00 ΔT=5 ms	Radii=45 and 135 m
PC4	Passive Circular	15	T=01:15:00 ΔT=5 ms	Radii=26 and 78 m
PT	Passive Triangular	16	T=01:53:00 ΔT=5 ms	Side=18.75, 37.5, 75, 150 and 300 m
PT2	Passive Large Triangular	4	T=02:02:00 ΔT=5 ms	Side=500 m
PL	Passive L_Shape	11	T=01:16:00 ΔT=5 ms	Distances=5, 10, 30, 60 and 100 m

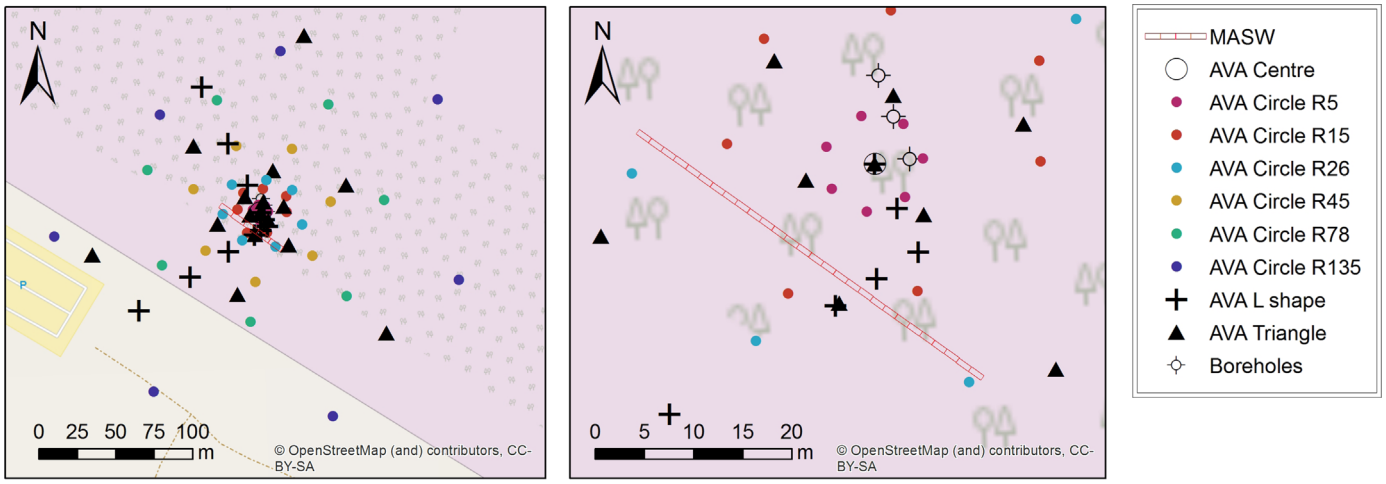

Fig. 14. Cadarache: map of the arrays. (Left) whole area interested by the acquisition. (Right) close-up view of the area. The largest triangular array is not shown.

good practice recommendations, which relate thickness of shallow layers and investigation depth to retrieved wavelengths in the experimental dispersion curve. Some analysts were able to reach frequency lower than the minimum frequency of Rayleigh wave fundamental mode thanks to the introduction of additional information such as the ellipticity and HVSR. Consistency between the natural frequency as estimated from the HVSR and the shear wave velocity profile can be considered valuable information to improve

Table 9
Cadarache: processing and inversion strategy for each team.

ID	Team	dataset	Surface wave mode	Additional information	dc processing	Inversion algorithm	Software
1	MU	PT, PT2	RE	HVSR	SPAC_directFit	LLS_EYE	mmspacfit
3	IST1	AV1, PC1, PC2, PC3, PC4	R0	HVSR	FK	NA_geopsy	Geopsy
4	UT	AV1, AV2, AH1, AH2, PC1, PC2, PC3, PC4, PT, PL	R0, L0		SPAC+FDBF	NA_geopsy	Geopsy
5	INGV	AV1, AV2, AH1, AH2, PC1, PC2, PC3, PC4, PT, PT2, PL	R0	HVSR	FK	NA_geopsy	Geopsy
7	Geom	AV1, PC1, PC2, PC4, PT, PT2	RE	HVSR	SPAC+PS	GA	Seisimager
10	TT	PT	R0		SPAC	SA-GA	
11	GV	AV1, AV2, PC1, PC2, PC3, PC4, PT, PT2	R0	HVSR	SPAC+PS	NLS	Seisimager; WinSASW
12	SED	PC1, PC2, PC3, PC4	R0, L0		3 CWD	NA_geopsy	Geopsy
13	PU	PC1, PC2, PC3, PC4	R0		SPAC+ FK	NA_geopsy	Geopsy
14	PT	AV1	R0, R1		FK+FDBF	MC	In-house

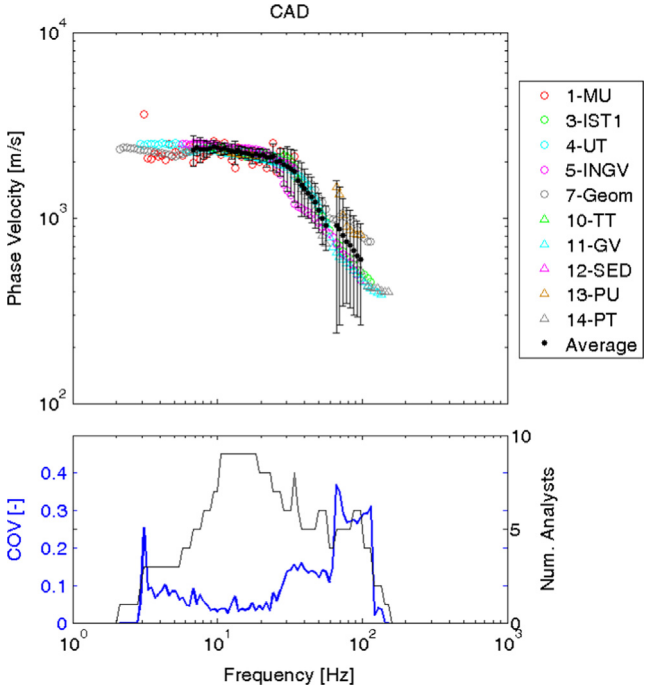

Fig. 15. Cadarache: (top) fundamental mode of Rayleigh wave dispersion curves. (bottom) Number of analyst and COV.

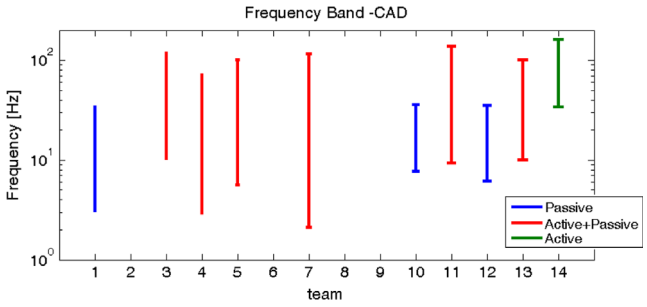

Fig. 16. Cadarache: frequency band associated with the retrieved dispersive curve or earth model interpretation.

the reliability of the model, a result which reinforces earlier findings by Arai and Tokimatsu [49], Hayashi et al. [94], Ikeda et al. [97] and Asten et al. [40].

Some teams constrained the inversions by exploiting as much as possible the information contained in the experimental data. In addition to HVSR and ellipticty, some teams estimated the P-wave velocity distribution by analysing the seismic refraction information contained in the active seismic datasets and from this result, it was possible to deduce the water table position and it helped to make more realistic assumptions on the Poisson's ratio.

The V_S profiles obtained at the three sites show some variability, but the consistency of the results is quite good with coefficient of variations among the provided solutions that are relatively low for a significant depth. Larger variability is observed at great depth, where the solutions approach the limits of applicability of the techniques because of the lack of constraint for the inverse problem.

Several teams adopted the same code for the inversion, i.e., the Neighborhood Algorithm implemented in Geopsy software package [38]. The variability of their results clearly shows the importance of some subjective choices (e.g., parameterization), and of the strategies (e.g., only fundamental Rayleigh waves) adopted by each analyst and the associated non-uniqueness issues.

Some features of the sites, like the bedrock interfaces in Mirandola and Cadarache, are not uniquely identified or not identified at all. For example the low-velocity layer in the upper 50 m of the Grenoble V_S profile is not detected by several teams (only 5 over 12 did). Larger variability is obtained at the depths where major interfaces are present (e.g., in Mirandola at a depth of about 25 m and a depth of about 100 m). This is a further demonstration of how much the non-uniqueness of the solution affects the reliability of the method. However, it is important to remark that, since it was a fully blind test, no a-priori information was provided to the teams. If we restrict the depth of interest for the comparisons, the accordance between results is indeed very encouraging.

In the Cadarache site, the differences among different results in terms of V_S profiles are larger than for Grenoble and Mirandola, at least within the first 20 m (Fig. 20). On the other side the observed variability is very small at intermediate depths. These trends may likely be justified considering that, because of weathering and fracturing, a significant lateral variability has to be expected for outcrop rock conditions as those of Cadarache. In addition, in a site like Cadarache, the variability observed in the shallow part could be also related to the fact that, since velocities are very high, a small variation in the wavenumber lead to large variation in estimated velocity. It is indeed important to remark that different teams used different subsets of experimental data. The expected lateral variability is clearly reflected in the experimental dispersion curves. This issue of spatial variability for rock outcrop is of paramount importance, because very often the reference sites of accelerometric networks on rock outcrops are characterized with surface-wave analysis. This inevitably involves a large volume of ground around the site of the reference station.

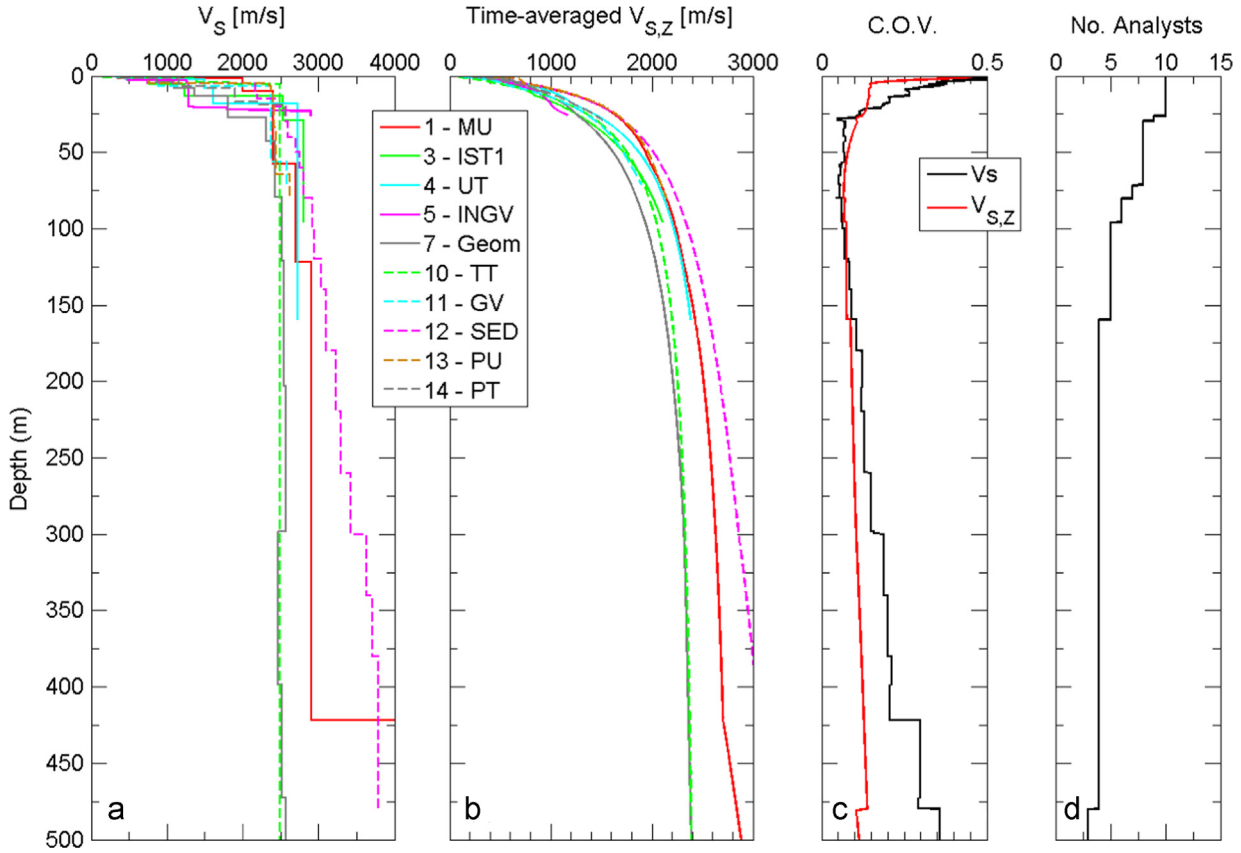

Fig. 17. Cadarache: (a) shear wave velocity profiles, (b) time-averaged V_S ($V_{S,Z}$) profiles, (c) CoV(V_s) and CoV($V_{S,Z}$) values, and (d) number of profiles.

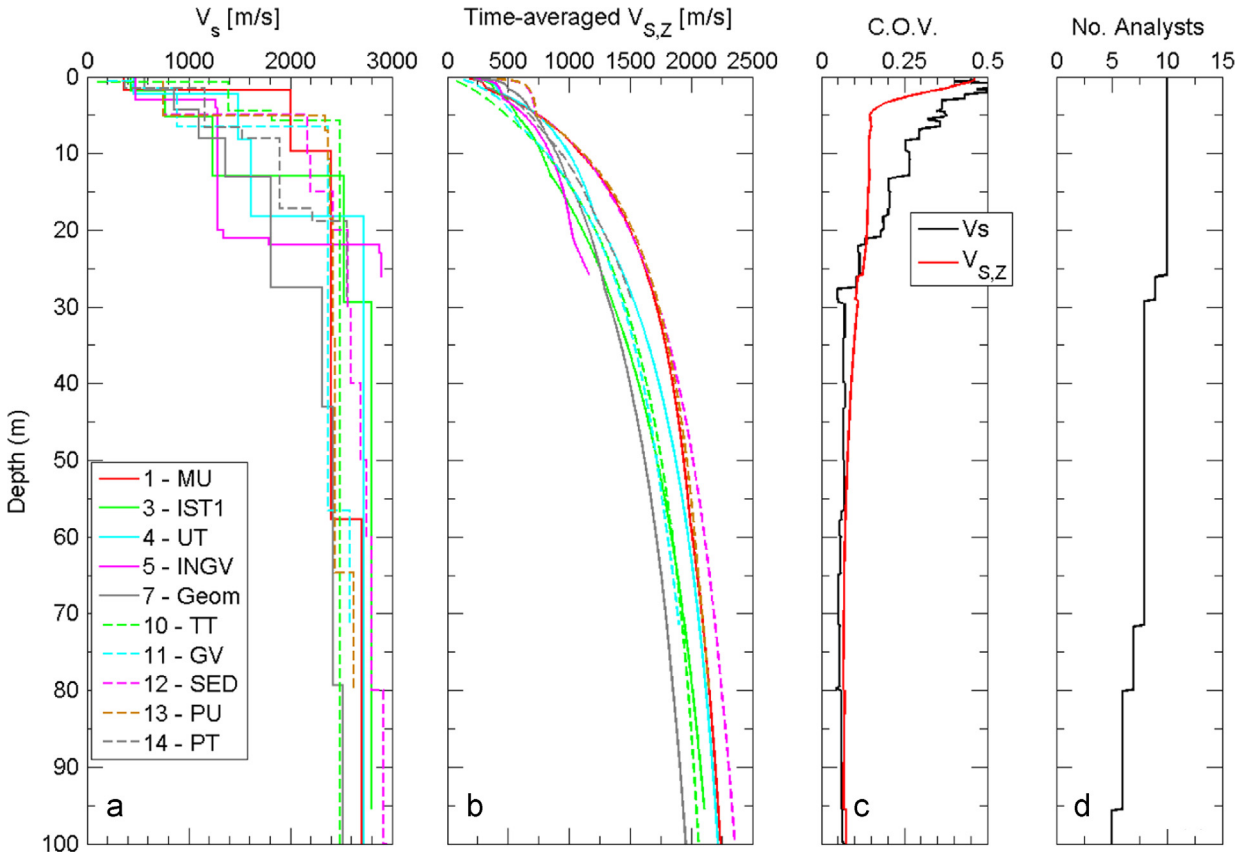

Fig. 18. Cadarache: close-up view of the top 100 m of Fig. 17.

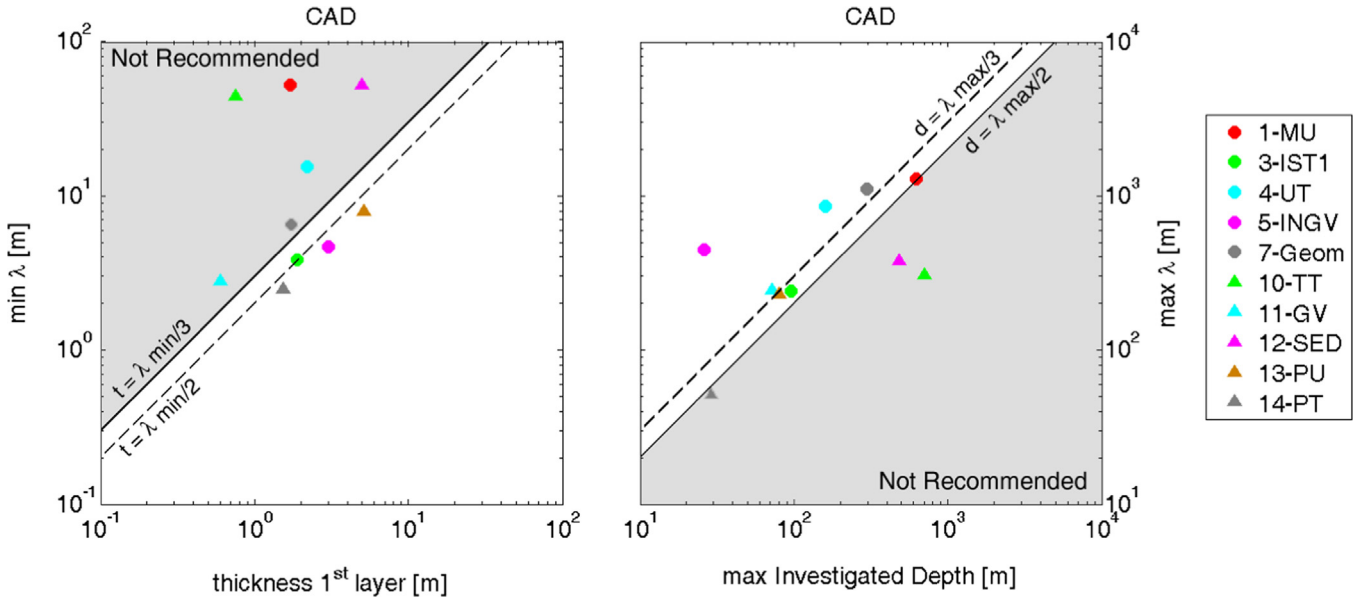

Fig. 19. Cadarache: (left) thickness of first layer as function of the minimum retrieved wavelength. (Right) maximum investigated depth as function of the maximum retrieved wavelength. In gray the "not-recommended" part of the domain.

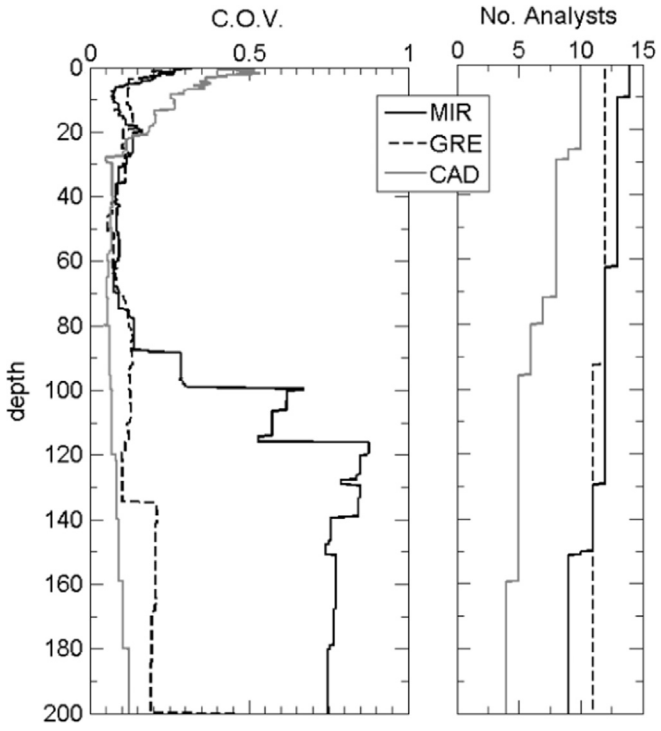

Fig. 20. CoV (left) and the number of analysts (right) related to the results in the three sites.

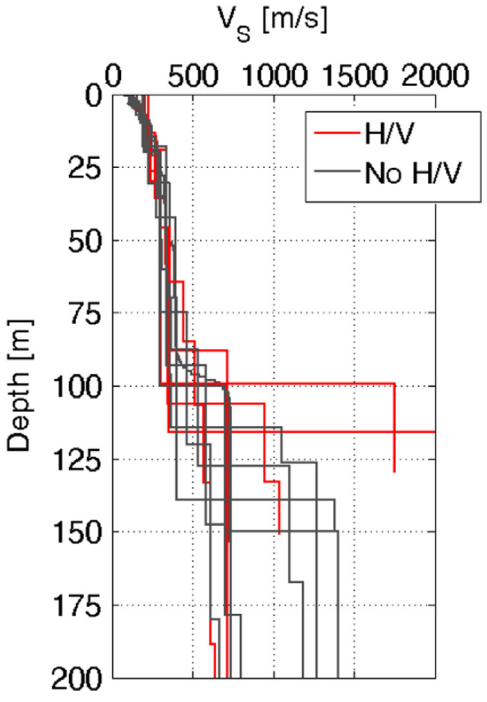

Fig. 21. Comparison between shear wave velocity profiles for Mirandola site (MIR) obtained accounting for the information retrieved from the HVSR (in red) and other profiles (in gray).

As far as the $V_{S,30}$ is concerned, in all the sites we obtained a variability quite comparable to each other independently from the subsoil conditions. This is a great proof of the reproducibility and repeatability of the surface-wave methods at least for the computation of $V_{S,30}$, which being a global parameter is less affected by solution non-uniqueness than local values of V_S at different depths (see also the examples reported by [98]).

5. Conclusions

The study was conducted in three sites with different subsoil conditions. In the blind test, the same raw data were available for different teams. Each team was free to adopt the strategy they considered the best to analyse surface-wave propagation. Agreement on the estimated dispersion curve was on average quite good for the three sites, confirming the robustness and precision of processing procedures. In all the three sites some features of subsoil were not uniquely identified and a certain variability of the results was observed in terms of V_S profiles. The variability of the V_S profiles was on average limited, with larger values in correspondence of relevant stratigraphic features, where the solution non-uniqueness limits the precision in identification of interface

Table 10
Some statistics about $V_{S,30}$: the mean value, the standard deviation (std), the coefficient of variation (CoV) and the ratio between the maximum and the minimum values of each group of results. Both the results calculated from the V_s profile (Inv) and from a direct estimate from the dispersion curve (dc) according to Brown et al. (2000) are reported.

$V_{S,30}$	MIR		GRE		CAD	
	Inv	dc	inv	dc	inv	dc
Mean [m/s]	219	227	364	381	1591	1561
Std [m/s]	16.4	7.55	14.7	7.71	168.5	142
CoV [-]	0.075	0.033	0.040	0.020	0.106	0.091
Max/min [-]	1.31	1.12	1.17	1.08	1.31	1.40

positions and hence a large variability in the results. The obtained results also confirm: the limited achievable resolution at depth; the influence of plausible lateral heterogeneities on the variability of the obtained results, as in the case of the rock outcrop site (Cadarache) of the present study. However, the overall variability can be considered quite low, provided that no a priori information was given to the teams to better constrain the inversion. These results confirm that the crucial aspect for uncertainties related to surface-wave analyses is the non-uniqueness of the solution of the inverse problem.

A-priori information (local geology, borehole logs) would have helped in better constraining the results, and in routine practice stratigraphic information from boreholes should be incorporated in order to improve the reliability. In addition, useful information for better constraining the inversion can be retrieved from further analysis of the available experimental data (e.g., with active-source data, analysis of critically refracted P-waves may provide an estimate of the water table and of the Poisson's ratio, while with passive data, the analysis of HVSR and Rayleigh ellipticity can provide useful information to improve the identification of the bedrock and/or sharp impedance contrasts).

Observed variability is more limited in the estimation of $V_{S,30}$, since this is an average parameter which is less influenced by the solution non-uniqueness than the estimates of individual layer thickness and V_S parameters.

Further developments of the InterPACIFIC research project will aim at identifying the role of different sources of variability, providing comprehensive and physics-based guidelines for surface-wave analysis.

Acknowledgments

The study has been financed by the Research and Development Program SIGMA funded by EdF (France), Areva (France), CEA (France) and ENEL (Italy) and by CASHIMA project, funded by CEA (France), ILL (France) and ITER (France). Partial funding for participants from the Politecnico di Torino was provided by the ReLUIS 2 project, sponsored by the Italian Civil Protection Agency. Partial funding for participants from the University of Texas was provided by U.S. National Science Foundation (NSF) Grant CMMI-1261775. However, any opinions, findings, and conclusions or recommendations expressed in this material are those of the authors and do not necessarily reflect the views of NSF.

Appendix A. Supporting information

Supplementary data associated with this article can be found in the online version at http://dx.doi.org/10.1016/j.soildyn.2015.12.010. These data include Google maps of the most important areas described in this article. All the experimental data collected at the three site for this study are available online at http://interpacific.geopsy.org.

References

[1] Kramer LS. Geotechnical earthquake engineering. Upper Saddle River, USA: Prentice-Hall; 1996.
[2] Boore DM. Can site response be predicted? J Earthq Eng 2004;8(1):1–41.
[3] CEN. EN 1998-1. Eurocode 8: design of structures for earthquake resistance. Brussels; 2004.
[4] BSSC. NEHRP Recommended provisions for the development of seismic regulations for new buildings, Building seismic safety council. Washington DC: Federal Emergency Management Agency; 2009.
[5] Abrahamson N, Atkinson G, Boore D, Bozorgnia Y, Campbell K, Chiou B, Idriss IM, Silva W, Youngs R. Comparisons of the NGA ground-motion relations. Earthq Spectra 2008;24(1):45–66. http://dx.doi.org/10.1193/1.2924363.
[6] Abrahamson N, Silva W. Summary of the Abrahamson and Silva NGA ground-motion relations. Earthq Spectra 2008;24(1):67–97. http://dx.doi.org/10.1193/1.2924360.
[7] Boore DM, Atkinson G. Ground-motion prediction equations for the average horizontal component of PGA, PGV, and 5%-damped PSA at spectral periods between 0.01 s and 10.0 s. Earthq Spectra 2008;24:99–138. http://dx.doi.org/10.1193/1.2830434.
[8] Chiou BS-J, Youngs R. An NGA model for the average horizontal component of peak ground motion and response spectra. Earthq Spectra 2008;24:173–215.
[9] Bard P-Y, Cadet H, Endrun B, Hobiger M, Renalier F, Theodulidis N, Ohrnberger M, Fäh D, Sabetta F, Teves-Costa P, Duval A-M, Cornou C, Guillier B, Wathelet M, Savvaidis A, Köhler A, Burjanek J, Poggi V, Gassner-Stamm G, Havenith HB, Hailemikael S, Almeida J, Rodrigues I, Veludo I, Lacave C, Thomassin S, Kristekova M. From non-invasive site characterization to site amplification: recent advances in the use of ambient vibration measurements. Geotech Geol Earthq Eng 2010;17:105–23.
[10] Socco LV, Foti S, Boiero D. Surface wave analysis for building near surface velocity models: established approaches and new prospectives. Geophysics 2010;75(5):A83–102.
[11] Foti S, Parolai S, Albarello D, Picozzi M. Application of Surface Wave Methods for Seismic site characterization. Surv Geophys 2011;32(6):777–825.
[12] Yong A, Martin A, Stokoe K, Diehl J. ARRA-funded VS30 measurements using multi-technique approach at strong-motion stations in California and Central-Eastern United States, U.S. Geological Survey Open-File Report 2013–1102. Reston, Virginia; 2013, p. 59.
[13] Foti S, Lai CG, Rix G, Strobbia C. Surface wave methods for near-surface site characterization. Boca Raton, FL, USA: CRC Press; 2014.
[14] Michel C, Edwards B, Poggi V, Burjánek J, Roten D, Cauzzi C, Fäh D. Assessment of site effects in Alpine regions through systematic site characterization of seismic stations. Bull Seism Soc Am 2014;104(6):2809–26.
[15] Cornou C, Ohrnberger M, Boore DM, Kudo K, Bard P-Y. Derivation of structural models from ambient vibration array recordings: results from an international blind test. In: ESG2006. vol. 2; 2009. p. 1127–1219.
[16] Cox BR, Wood CM, Teague DP. Synthesis of the UTexas1 surface wave dataset blind-analysis study: inter-analyst dispersion and shear wave velocity uncertainty. In: Geo-Congrees. Atlanta Georgia; 2014.
[17] Parolai S, Richwalski SM, Milkereit C, Fäh D. S-wave velocity profiles for earthquake engineering purposes for the Cologne area (Germany). Bull Earthq Eng 2006;4(1):65–94.
[18] Cercato M. Addressing non-uniqueness in linearized multichannel surface wave inversion. Geophys Prospect 2009;57(1):27–47.
[19] Foti S, Comina C, Boiero D, Socco LV. Non uniqueness in surface wave inversion and consequence on seismic site response analyses. Soil Dyn Earthq Eng 2009;29:982–93.
[20] Picozzi M, Strollo A, Parolai S, Durukal E, Ozel O, Karabulut S, Zschau J, Erdik M. Site characterisation by seismic noise in Istanbul. Soil Dyn Earthq Eng 2009;29:469–82.
[21] Molnar S, Dosso SE, Cassidy JF. Bayesian inversion of microtremor array dispersion data in southwestern British Columbia. Geophys J Int 2010;183(2):923–40.
[22] Renalier F, Jongmans D, Savvaidis A, Wathelet M, Endrun B, Cornou C. Influence of parameterization on inversion of surface wave dispersion curves and definition of an inversion strategy for sites with a strong Vs contrast. Geophysics 2010;75(6):B197–209.
[23] Boaga J, Vignoli G, Cassiani G. Shear wave profiles from surface wave inversion: the impact of uncertainty on seismic site response analysis. J Geophys Eng 2011;8(2):162.
[24] Dettmer J, Molnar S, Steininger G, Dosso SE, Cassidy JF. Trans-dimensional inversion of microtremor array dispersion data with hierarchical autoregressive error models. Geophys J Int 2012;188(2):719–34.
[25] Di Giulio G, Savvaidis A, Ohrnberger M, Wathelet M, Cornou C, Knapmeyer-Endrun B, Renalier F, Theodoulidis N, Bard P-Y. Exploring the model space and ranking a best class of models in surface wave dispersion inversion: application at European strong-motion sites. Geophysics 2012;77(3):B1147–66.
[26] Aki K. Space and time spectra of stationary stochastic waves with special reference to microtremors. Bull Earth Res Inst Tokio Univ 1957;25:415–57.

[27] Capon J. High-resolution frequency-wavenumber spectrum analysis. Proc IEEE 1969;57(8):1408–18.
[28] Lacoss RT, Kelly EJ, Toksöz MN. Estimation of seismic noise structure using arrays. Geophysics 1969;34:21–38.
[29] Nolet P, Panza GF. Array analysis of seismic surface waves: limits and possibilities. Pure Appl Geophys 1976;114:776–90.
[30] McMechan GA, Yedlin MJ. Analysis of dispersive wave by wave field transformation. Geophysics 1981;46:868–74.
[31] Park CB, Miller RD, Xia J. Multichannel analysis of surface waves. Geophysics 1999;64(3):800–8.
[32] Rothman DH. Nonlinear inversion, statistical mechanics, and residual statics estimation. Geophysics 1985;50:2784–96.
[33] Herrmann RB. Surface wave inversion. Computer programs in seismology. Saint Louis, USA: Saint Louis University; 1987. p. 4.
[34] Yamanaka H, Ishida H. Application of genetic algorithms to an inversion of surface-wave dispersion data. Bull Earthq Eng 1996;86:436–44.
[35] Lai CG. Simultaneous inversion of rayleigh phase velocity and attenuation for near-surface site characterization (Ph.D. thesis). Atlanta, Georgia, USA: Georgia Institute of Technology; 1998.
[36] Xia J, Miller RD, Park CB. Estimation of near-surface shear-wave velocity by inversion of Rayleigh waves. Geophysics 1999;64:691–700.
[37] Socco LV, Boiero D. Improved Monte Carlo inversion of surface wave data. Geophys Prospect 2008;56:357–71.
[38] Wathelet M. An improved neighborhood algorithm: parameter conditions and dynamic scaling. Geophys Res Lett 2008;35:L09301.
[39] Maraschini M, Foti S. A Monte Carlo multimodal inversion of surface waves. Geophys J Int 2010;182(3):1557–66.
[40] Asten M, Askan A, Ekincioglu EE, Sisman FN, Ugurhan B. Site characterization in Northwestern Turkey based on SPAC and HVSR analysis of microtremor noise. Explor Geophys 2014;45:74–85. http://dx.doi.org/10.1071/EG12026.
[41] Tran KT, Hiltunen DR. An assessment of surface wave techniques at the Texas A&M national geotechnical experimentation site. In: Juang CH, et al., editors. GeoRisk 2011: geotechnical risk assessment and management, 224. ASCE GSP; 2011. p. 859–66.
[42] Kim DS, Park HJ, Bang ES. Round robin test for comparative study of in-situ seismic tests. In: Mayne RQ, Coutinho PW, editors. Geotechnical and geophysical site characterization, 4. Leiden (NL): CRC Press; 2012. p. 1427–34.
[43] Garofalo F, Foti S, Hollender F, Bard P-Y, Cornou C, Cox BR, Dechamp A, Ohrnberger M, Perron V, Sicilia D, Teague D, Vergniault C. Interpacific project: comparison of invasive and non-invasive methods for seismic site characterization, part II: inter-comparison between surface-wave and borehole methods. Soil Dyn Earthq Eng 2016. http://dx.doi.org/10.1016/j.soildyn.2015.12.009.
[44] Anzidei M, Maramai A, Montone P. The Emilia (northern Italy) seismic sequence of May–June, 2012: preliminary data and results. Ann Geophys 2012;55(4):515–842. http://dx.doi.org/10.4401/ag-6232 Special Issue.
[45] Guéguen P, Cornou C, Garambois S, Banton J. On the limitation of the H/V spectral ratio using seismic noise as an exploration tool. Application to the Grenoble basin (France). PAGEOPH 2007;164:1–20. http://dx.doi.org/10.10007/s00024-006-0151-x.
[46] Aki K, Richard PG. Quantitative seismology: theory and methods, 2nd edition. Sausalito, CA, USA: University Science Books; 1980.
[47] Tokimatsu K. Geotechnical site characterisation using surface waves. In: Proceedings of the first Int. Conf. Earth Geotech. Eng.. Is-Tokyo; 1995. p. 36.
[48] Foti S. Multistation methods for geotechnical characterization using surface waves (Ph.D. thesis). Polite- di Torino, Turin, Italy; 2000.
[49] Arai H, Tokimatsu K. S-wave velocity profiling by joint inversion of microtremor dispersion curve and horizontal-to-vertical (H/V) spectrum. Bull Seism Soc Am 2005;95:1766–78.
[50] Ikeda T, Matsuoka T, Tsuji T, Hayashi K. Multimode inversion with amplitude response of surface waves in the spatial autocorrelation method. Geophys J Int 2012;190:541–52.
[51] Stokoe II KH, Wright SG, Bay J, Roesset JM. Characterization of geotechnical sites by SASW method. In: Woods RD, editor. Geophysical characterization of sites. Oxford, UK: Oxford & IBH Publ; 1994. p. 15–25.
[52] Socco LV, Strobbia C. Surface-wave method for near-surface characterisation: a tutorial. Surf Geophys 2004;2:165–85.
[53] Sambuelli L, Deidda GP. Swyphone™: a new seismic sensor with increased response to sh-waves. In: Proceedings of fifth meeting of environmental and engineering geophysical society. Budapest; 6-9 Sept 1999.
[54] Foti S, Sambuelli L, Socco LV, Strobbia C. Experiments of joint acquisition of seismic refraction and surface wave data. Surf Geophys 2003;1(3):119–29.
[55] Johnson DJ, Dudgeon DE. Array signal processing-concepts and techniques. In: Oppenheim Alan v, editor. Prentice hall signal processing series. Upper Saddle River, NJ, USA: PTR Prentice Hall; 1993.
[56] Rost S, Thomas C. Array seismology: methods and applications. Rev Geophys 2002;40(3):2-1–27. http://dx.doi.org/10.1029/2000RG000100.
[57] Okada H. The microtremor survey method. Geophysical Monograph series, 12. Tulsa, OK, USA: Society of Exploration Geophysics; 2003.
[58] Maranò S, Fäh D, Lu YM. Sensor placement for the analysis of seismic surface waves: Sources of error, design criterion and array design algorithms. Geophys J Int 2014;197(3):1566–81.
[59] Louie JN. Faster, better: shear-wave velocity to 100 m depth from refraction microtremor arrays. Bull Seism Soc Am 2001;91(2):347–64.
[60] Cox BR, Beekman AN. Intramethod variability in remi dispersion measurements and vs estimates at shallow bedrock sites. J Geotech Geoenviron Eng 2010;137(4):354–62.
[61] Strobbia C, Cassiani G. Refraction microtremors: data analysis and diagnostics of key hypotheses. Geophysics 2011;76(3):MA11–20.
[62] Asten M. On bias and noise in passive seismic data from finite circular array data processed using SPAC methods. Geophysics 2006;71(6):V153–62. http://dx.doi.org/10.1190/1.2345054.
[63] Forbriger T. Inversion of shallow-seismic wavefield: I Wavefield transformation. Geophys J Int 2003;153:719–34.
[64] Fäh D, Kind F, Giardini D. Inversion of local S-wave velocity structures from average H/V ratios, and their use for the estimation of site-effects. J Seism 2003;7:449–67.
[65] Hobiger M, Bard P-Y, Cornou C, Le Bihan N. Single station determination of Rayleigh wave ellipticity by using the random decrement technique (RayDec). Geophys Res Lett 2009;36:L14303.
[66] Poggi V, Fäh D. Estimating Rayleigh wave particle motion from three-component array analysis of ambient vibrations. Geophys J Int 2010;180(1):251–67.
[67] Poggi V, Fäh D, Burjanek J, Giardini D. The use of Rayleigh wave ellipticity for site-specific hazard assessment and microzonation. An application to the city of Luzern (Switzerland). Geophys J Int 2012;188(3):1154–72.
[68] Zywicki DJ. Advanced signal processing methods applied to engineering analysis of seismic surface waves. Georgia, Atlanta: Georgia Institute of technology; 1999.
[69] Bettig B, Bard P-Y, Scherbaum F, Riepl J, Cotton F, Cornou C, Hatzfeld D. Analysis of dense array noise measurements using the modified spatial auto-correlation method (SPAC): application to the Grenoble area. Boll di Geofis Teor Ed Appl 2001;42(3–4):281–304.
[70] Maranò S, Reller C, Loeliger H-A, Fäh D. Seismic wave estimation and wavefield decomposition: application to ambient vibrations. Geophys J Int 2012;191(1):175–88.
[71] Nazarian S. In situ determination of elastic moduli of soil deposits and pavement system by spectral-analysis-of-surface-waves method. Austin, USA: University of Texas; 1984.
[72] Foti S, Strobbia C. Some notes on model parameters for surface wave data inversion. In: Proceedings Of SAGEEP. Las Vegas, USA; 2002.
[73] Luke B, Calderòn-Macìas C, Stone RC, Huynh M. Nonuniqueness in inversion of seismic surface-wave data. In: Proceedings on the symposium on the application of geophysics to engineering and environmental problems. 2003.
[74] Picozzi M, Albarello D. Combining Genetic and Linearized algorithms for a two-step joint inversion of Rayleigh wave dispersion and H/V spectral ratio curves. Geophys J Int 2007;169(1):189–200.
[75] Foti S, Parolai S, Bergamo P, Di Giulio G, Maraschini M, Milana G, Picozzi M, Puglia R. Surface wave surveys for seismic site characterization of accelerometric stations in ITACA. Bull Earthq Eng 2011;9(6):1797–820. http://dx.doi.org/10.1007/s10518-011-9306-y.
[76] Forbriger T. Inversion of shallow-seismic wavefields: II Inferring subsurface. Geophys J Int 2003;153:735–52.
[77] O'Neill A, Matsuoka T. Dominant higher surface-wave modes and possible inversion pitfalls. J Environ Eng Geophys 2005;10(2):185–201.
[78] Beaty KS, Schmitt DR, Sacchi M. Simulated annealing inversion of multimode Rayleigh wave dispersion curves for geological structure. Geophys J Int 2002;151:622–31.
[79] Feng S, Sugiyama T, Yamanaka H. Effectiveness of multimodel surface wave inversion in shallow engineering site investigation. Explor Geophys 2005;36:26–33.
[80] Dal Moro G, Pipan M, Gabrielli P. Rayleigh wave dispersion curve inversion via genetic algorithms and marginal posterior probability density estimation. J Appl Geophys 2007;61:39–55.
[81] Socco LV, Boiero D, Foti S, Wisén R. Laterally constrained inversion of ground roll from seismic reflection records. Geophysics 2009;74(6):35–45.
[82] Xia J, Miller RD, Park CB, Tian G. Inversion of high frequency surface waves with fundamental and higher modes. J Appl Geophys 2003;52(1):45–57.
[83] Parolai S, Picozzi M, Richwalski SM, Milkereit C. Joint inversion of phase velocity dispersion and H/V ratio curves from seismic noise recordings using a genetic algorithm, considering higher modes. Geophys Res Lett 2005;32:L01303.
[84] Dal Moro G, Ferigo F. Joint analysis of Rayleigh-and Love-wave dispersion: issues, criteria and improvements. J Appl Geophys 2011;75(3):573–89.
[85] Hobiger M, Cornou C, Wathelet M, Di Giulio G, Knapmeyer-Endrun B, Renalier F, Bard P-Y, Savvaidis A, Hailemikael S, Le Bihan N, Ohrnberger M, Theodoulidis M. Ground structure imaging by inversions of Rayleigh wave ellipticity: sensitivity analysis and application to European strong-motion sites. Geophys J Int 2013;192(1):207–29. http://dx.doi.org/10.1093/gji/ggs005.
[86] Asten MW, Dhu T, Lam N. Optimised array design for microtremor array studies applied to site classification; observations, results and future use. In: Proceedings of the thirteenth World Conference of Earthquake Engineering. Vancouver; 2004. Paper 2903.
[87] Wathelet M, Jongmans D, Ohrnberger M. Direct inversion of spatial auto-correlation curves with the neighbourhood algorithm. Bull Seism Soc Am 2005;95:1787–800.
[88] Nogoshi M, Igarashi T. On the amplitude characteristics of microtremor, Part II. J Seism Soc Jpn 1971;24:26–40.

[89] Nakamura Y. A method for dynamic characteristics estimations of subsurface using microtremors on the ground surface. Railw Tech Res Inst Q Rep 1989;30 (1):25–33.
[90] Hayashi K. Analysis of surface-wave data including higher modes using the genetic algorithm. Proc GeoCongress. 2012.
[91] Yamanaka H. Inversion of surface-wave phase velocity using hybrid heuristic search method. Butsuri-tansa (Geophys Explor) 2007;60:265–75.
[92] Joh SH. Advances in interpretation and analysis techniques for spectral-analysis-of-surface-waves (SASW) measurements. Department of civil, architectural, and environmental engineering. Austin, TX: University of Texas; 1996. p. 240 Ph.D. Dissertation.
[93] Abbiss C. Shear wave measurements of the elasticity of the ground. Geotechnique 1981;31:91–104.
[94] Hayashi K, Nozu A, Tanaka M. Joint inversion of three component microtremor measurements and microtremor array measurements at Mexico City. SEG Technical Program Expand Abstracts. 2011, p. 17–921.
[95] Boore DM, Brown LT. Comparing shear-wave velocity profiles from inversion of surface-wave phase velocities with downhole measurements: systematic differeneces between the CXW method and downhole measurements at six USC strong-motion sites. Seismol Res Lett 1998;69(3):222–9.
[96] Brown LT, Diehl JG, Nigbor RL. A simplified procedure to measure average shear-wave velocity to a depth of 30 m (Vs30). In: Proceedings of the twelfth world conferance on earthquake engineering, society of earthquake engineering. Auckland, New Zealand; 2000.
[97] Ikeda T, Asten MW, Matsuoka T. Joint inversion of spatial autocorrelation curves with HVSR for site characterization in Newcastle. In: Proceedings of 23rd ASEG international geophysical conference and exhibition. Extended Abstracts. Melbourne, Australia; 2013. p. 1–4.
[98] Comina C, Foti S, Boiero D, Socco LV. Reliability of $V_{S,30}$ evaluation from surface-wave tests. J Geotech Geoenviron Eng 2011;137(6):579–86.